
Tracing Hyperparameter Dependencies for Model Parsing via Learnable Graph Pooling Network

Xiao Guo, Vishal Asnani, Sijia Liu, Xiaoming Liu
Michigan State University
{guoxia11, asnanivi, liusiji5, liuxm}@msu.edu

Abstract

Model Parsing defines the task of predicting hyperparameters of the generative model (GM), given a GM-generated image as the input. Since a diverse set of hyperparameters is jointly employed by the generative model, and dependencies often exist among them, it is crucial to learn these hyperparameter dependencies for improving the model parsing performance. To explore such important dependencies, we propose a novel model parsing method called Learnable Graph Pooling Network (LGPN), in which we formulate model parsing as a graph node classification problem, using graph nodes and edges to represent hyperparameters and their dependencies, respectively. Furthermore, LGPN incorporates a learnable pooling-unpooling mechanism tailored to model parsing, which adaptively learns hyperparameter dependencies of GMs used to generate the input image. Also, we introduce a Generation Trace Capturing Network (GTC) that can efficiently identify generation traces of input images, enhancing the understanding of generated images’ provenances. Empirically, we achieve state-of-the-art performance in model parsing and its extended applications, showing the superiority of the proposed LGPN. The source code is available at [link](#).

1 Introduction

Generative Models (GMs) [22, 71, 11, 42, 33, 58, 32, 34, 48], *e.g.*, Generative Adversarial Networks (GANs), Variational Autoencoder (VAEs), and Diffusion Models (DMs), have gained significant attention, offering remarkable capabilities in generating visually compelling images. However, the proliferation of such Artificial Intelligence Generated Content (AIGC) can inadvertently propagate inaccurate or biased information. To mitigate such negative impact, various image forensics [50] methods have been proposed [60, 52, 20, 6, 24, 62, 31, 74, 54, 69, 1]. Alongside these defensive efforts, the recent work [2] defines a novel research topic called “*model parsing*”, which predicts 37 GM hyperparameters using the generated image as the input, as detailed in Fig. 1a.

Model parsing requires analyzing GM hyperparameters and gaining insights into origins of generated images, which facilitate defenders to develop effective countermeasures. For example, one can reasonably determine if there exists coordinated attacks [2] — two images are generated from the same GM that is *unseen* during the training, using predicted hyperparameters from the model parsing algorithm. In light of this, the previous method [2] introduces a clustering-based approach that achieves effective model parsing performance. However, this approach neglects the learning of hyperparameter dependencies. For instance, an inherent dependency exists between GM’s layer number and parameter number, as GM’s layer number is positively proportional to its parameter number. A similar proportional relationship exists between the number of convolutional layers and convolutional filters. In contrast, the use of the L1 loss is negatively correlated with the use of the L2 loss, as GMs typically do not employ both losses as objective functions simultaneously. We believe the neglect of such dependencies might cause a suboptimized performance. Therefore, in

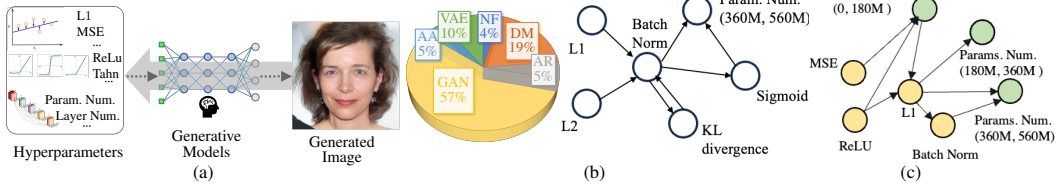


Figure 1: (a) Hyperparameters define a GM that generates images. *Model parsing* [2] refers to the task of predicting hyperparameters given the generated image. (b) We study the co-occurrence pattern among different hyperparameters in various GMs from the RED140 dataset whose composition is shown as the pie chart¹, and subsequently construct a directed graph to capture dependencies among these hyperparameters. (c) We define the discrete-value graph node (yellow) (e.g., L1 and Batch Norm) for each discrete hyperparameter. For each continuous hyperparameter (green), we partition its range into n distinct intervals, and each interval is then represented by a graph node: Parameter Number has three corresponding continuous-value graph nodes. Representations on these graph nodes are used to predict hyperparameters.

this work, we propose to use graph nodes and edges to explicitly represent hyperparameters and their dependencies, respectively, and then propose a model parsing algorithm that utilizes the effectiveness of Graph Convolution Network (GCN) [35, 59, 18, 49] in capturing dependencies among graph nodes.

Specifically, we first use training samples in the RED dataset [2] to construct a directed graph (Fig. 1b). The directed graph, based on the label co-occurrence pattern, illustrates the fundamental correlation between different categories and helps prior GCN-based methods achieve remarkable performances in various applications [10, 7, 66, 44, 16, 56]. In this work, this directed graph is tailored to the model parsing — we define discrete-value and continuous-value graph nodes to represent hyperparameters, shown in Fig. 1c. Then, we use this graph to formulate model parsing as a graph node classification problem, in which the discrete-value graph node feature decides if a given hyperparameter is used in the given GM, and the continuous-value node feature decides which range the hyperparameter resides. This formulation helps obtain effective representations of hyperparameters and dependencies among them for the model parsing task, detailed in Sec. 3.1.

To this end, we propose a novel model parsing framework called Learnable Graph Pooling Network (LGPN), which contains a Generation Trace Capturing Network (GTC) and a GCN refinement block (Fig. 2). Our GTC differs from neural network backbones used in State-of-The-Art (SoTA) forgery detection methods [60, 72, 61, 4, 61], using down-sampling operations (e.g., pooling) gradually reduce the learned feature map resolution during the forward propagation. This down-sampling can cause the loss of already subtle generation traces left by GMs. Instead, our GTC leverages a high-resolution representation that largely preserves generation traces throughout the forward propagation (Sec. 3.2.1). Therefore, the learned image representation from the GTC deduces crucial information (i.e., generation trace) of used GMs and benefits model parsing. Subsequently, this representation is transformed into a set of graph node features, along with the pre-defined directed graph, which are fed to the GCN refinement block. The GCN refinement block contains trainable pooling layers that progressively convert the correlation graph into a series of coarsened graphs by merging original graph nodes into supernodes. Then, the graph convolution is conducted to aggregate node features at all levels of graphs, and trainable unpooling layers are employed to restore supernodes to their corresponding children nodes. This learnable pooling-unpooling mechanism helps LGPN generalize to parsing hyperparameters in unseen GMs and improves the GCN representation learning. In summary, our contributions are:

- ◊ We innovatively formulate *model parsing* as a graph node classification problem, using a directed graph to help capture hyperparameter dependencies for better model parsing performance.
- ◊ A learnable pooling-unpooling mechanism is introduced with GCN to enhance representation learning in model parsing and its generalization ability.
- ◊ We propose a Generation Trace Capturing Network (GTC) that utilizes high-resolution representations to capture generation traces, facilitating a deeper understanding of the image’s provenance.

¹We adhere to naming conventions from the previous work [2], as the pie chart of Fig. 1b, where AA, AR, and NF represent Adversarial Attack models, Auto-Regressive models, and Normalizing Flow models, respectively.

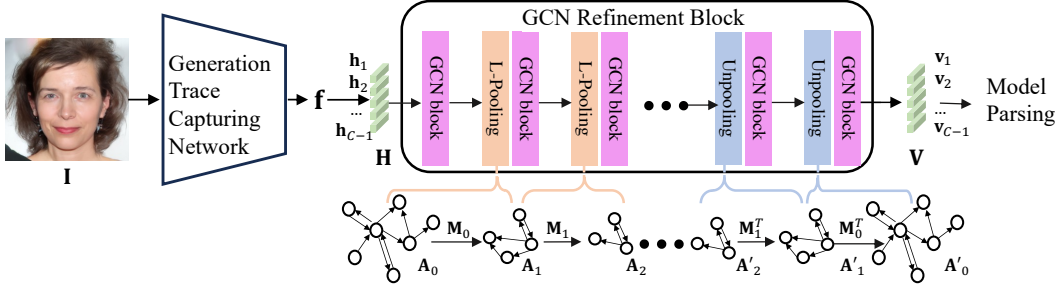


Figure 2: **Learnable Graph Pooling Network.** Given an input image I , the proposed LGPN first uses the Generation Trace Capturing Network (Fig. 3) to extract the representation f . Then, f is transformed into H , which represents a set of graph node features and is fed into the GCN refinement block. The GCN refinement block stacks GCN layers with paired pooling-unpooling layers (Sec. 3.2.2) and produces the refined feature V for model parsing. Our method is jointly trained with 3 different objective functions (Sec. 3.3).

◊ Extensive empirical results demonstrate the SoTA performance of the proposed LGPN in model parsing and identifying coordinated attacks. Additionally, the GTC’s effectiveness is validated through CNN-generated image detection and image attribution tasks.

2 Related Works

Model Parsing Previous model parsing works [57, 30, 17, 3, 45] require prior knowledge of machine learning models and their inputs to predict model hyperparameters, and such predictions are primarily limited to architecture-related hyperparameters [17, 45]. In contrast, Asnani *et al.* [2] recently propose a technique to estimate 37 pre-defined hyperparameters covering loss functions and architectures by only leveraging generated images as inputs. Specifically, this work [2] designs FEN-PN that uses a clustering-based approach to estimate the mean and standard deviation of hyperparameters for network architecture and loss function types. Then, FEN-PN uses a fingerprint estimation network that is trained with four constraints to estimate the fingerprint for each image. These fingerprints are employed to predict hyperparameters. However, FEN-PN overlooks dependencies among hyperparameters, which cannot be adequately captured by the estimated mean and standard deviation. In contrast, we propose LGPN, using GCN to model dependencies among different hyperparameters, improving overall model parsing performance.

GCN-based Method Graph Convolution Neural Network (GCN) shows effectiveness in encoding dependencies among different graph nodes [35, 59, 18, 26, 28], and in the computer vision community, directed graphs based on label co-occurrence patterns are used with GCN in tasks such as multi-label image recognition [10, 7, 66], semantic segmentation [9, 29, 39, 16], and person ReID and action localization [44, 63, 8, 56]. These works rely on original graph structures, whereas our method uses a pooling algorithm to modify this graph structure, which can benefit GCN’s representation learning. Also, our GCN refinement block differs from Graph U-Net [19] in that it reduces the graph size by removing certain nodes. However, we formulate model parsing as a graph node classification task, where each node represents a specific hyperparameter, meaning no nodes should be discarded.

Learning Image Generation Traces GMs leave particular traces in their generated images [41, 12], which can be visual artifacts [70, 4] or through evident peaks in the frequency domain [72, 60]. These traces serve as important clues for image forensic tasks such as detection [12, 72, 60], attribution [68, 47] and model parsing [2, 64, 65, 21]. Current methods [60, 72, 61, 4, 61, 55] use backbones like ResNet and XceptionNet that have high generalization abilities, and vision-language foundation models [53, 73, 23] also show effectiveness in detecting unseen forgeries. However, these prior methods often use backbones that rely on downsampling operations, such as convolutions with large strides and pooling, which capture global semantics but discard high-frequency details that contain critical generation traces. In contrast, we propose a Generation Trace Capturing network that mainly operates on a high-resolution representation for capturing such generation traces. Its effectiveness is shown in our experiment by comparing against recent detection methods that use pre-trained CLIP features [46] and the novel representation [61], and competitive image attribution methods.

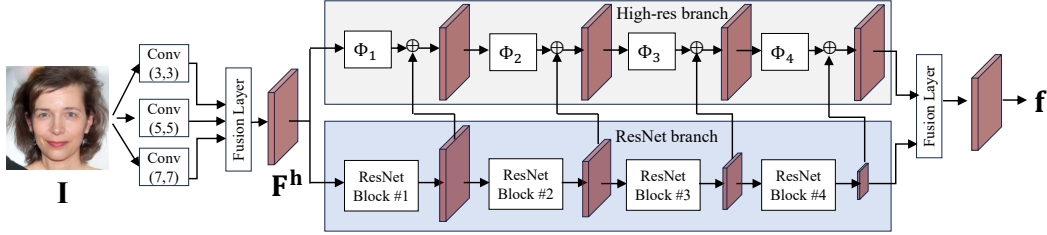


Figure 3: **Generation Trace Capturing Network**. First, convolution layers with different kernel sizes extract feature maps of the input image \mathbf{I} . A fusion layer concatenates these feature maps and then proceeds the concatenated feature to the ResNet branch and High-res branch.

3 Method

In this section, we first revisit some fundamental preliminaries in Sec. 3.1, and then introduce the proposed Learnable Graph Pooling Network (LGPN) in Sec. 3.2. Lastly, we describe training and inference procedures in Sec. 3.3.

3.1 Preliminaries

This section provides the problem statement of *model parsing* and its formulation as a graph node classification task with the Graph Convolutional Network (GCN).

Revisiting Model Parsing Given an input image $\mathbf{I} \in \mathbb{R}^{3 \times W \times H}$ generated by a GM (*i.e.*, \mathcal{G}), the model parsing algorithm generates three vectors ($\mathbf{y}^d \in \mathbb{R}^{18}$, $\mathbf{y}^c \in \mathbb{R}^9$ and $\mathbf{y}^l \in \mathbb{R}^{10}$) as predictions of C hyperparameters used in the \mathcal{G} . Specifically, defined by the previous work [2], these predictable C hyperparameters include discrete and continuous architecture hyperparameters, as well as loss functions, which are denoted as \mathbf{y}^d , \mathbf{y}^c , and \mathbf{y}^l , respectively. For \mathbf{y}^d and \mathbf{y}^l , each element is a binary value representing if the corresponding feature is used or not. Each element of \mathbf{y}^c is the value of certain continuous architecture hyperparameters, such as the layer number and parameter number. As these hyperparameters are in different ranges, we normalize them into $[0, 1]$, same as the previous work [2]. Predicting \mathbf{y}^d and \mathbf{y}^l is a classification task while the regression is used for \mathbf{y}^c . Detailed definitions are in Tab. 4, 5, and 6 of the supplementary. We augment the previous model parsing dataset (*e.g.*, RED116 [2]) with different diffusion models such as DDPM [27], ADM [15] and Stable Diffusions [48], increasing the spectrum of GMs. Also, we add real images on which these GMs are trained into the dataset. In the end, we collect 140 GMs in total and denote such a collection as the RED140 dataset. Details are in the Supplementary Sec. D.

Correlation Graph Construction We design a graph structure of model parsing, where graph nodes and edges represent hyperparameters and their dependencies, respectively. We first use conditional probability $P(L_j|L_i)$ to denote the probability of hyperparameter L_j occurrence when hyperparameter L_i appears. We count the occurrence of such pairs in the RED140 to construct the matrix $\mathbf{G} \in \mathbb{R}^{C \times C}$, and \mathbf{G}_{ij} denotes the conditional probability of $P(L_j|L_i)$. We apply a fixed threshold τ to remove edges with low correlations. Therefore, we obtain a directed graph $\mathbf{A} \in \mathbb{R}^{C \times C}$, in which \mathbf{A}_{ij} indicates if there exists an edge between node i and j .

Specifically, as depicted in Fig. 1c, each discrete hyperparameter (*e.g.*, discrete architecture hyperparameters and loss functions) is represented by one graph node, denoted as a discrete-value graph node. For continuous hyperparameters, we first divide its value range into n different intervals, and each of the intervals is represented by one graph node, termed a continuous-value graph node. Subsequently, we use discrete-value graph nodes to decide if given hyperparameters are present, and the continuous-value node decides which range the hyperparameter resides. Therefore, we denote the constructed graph as \mathbf{A} and apply stacked graph convolution on \mathbf{A} as following:

$$\mathbf{h}_i^l = \text{ReLU}\left(\sum_{j=1}^N \mathbf{A}_{i,j} \mathbf{W}^l \mathbf{h}_j^{l-1} + \mathbf{b}^l\right), \quad (1)$$

where \mathbf{h}_i^l represents the i -th node feature in graph \mathbf{A} . \mathbf{W}^l and \mathbf{b}^l are weight and bias terms.

3.2 Learnable Graph Pooling Network

In this section, we detail the Generation Trace Capturing Network (GTC) and GCN refinement block—two major components used in the proposed LGPN, as depicted in Fig. 2.

3.2.1 Generation Trace Capturing Network

As shown in Fig. 3, GTC uses one branch (*i.e.*, ResNet branch) to propagate the original image information. Meanwhile, the other branch, denoted as *high-res branch*, harnesses the high-resolution representation that helps detect high-frequency generation artifacts stemming from various GMs. More formally, three separate 2D convolution layers with different kernel sizes (*e.g.*, 3×3 , 5×5 and 7×7) are utilized to extract feature maps of \mathbf{I} . We concatenate these feature maps and feed them to the fusion layer — the 1×1 convolution for the channel dimension reduction. Then, we obtain the feature map $\mathbf{F}^h \in \mathbb{R}^{D \times W \times H}$, with the same resolution as \mathbf{I} . After that, we proceed \mathbf{F}^h to a dual-branch backbone. Specifically, we upsample intermediate features output from each ResNet block and incorporate them into the high-res branch, as depicted in Fig. 3. The high-res branch also has four different convolution blocks (*e.g.*, Φ_b with $b \in \{1 \dots 4\}$), which do not employ down-sampling operations, such as the 2D convolution with large strides or pooling layers. Then, intermediate feature maps throughout the high-res branch possess the same resolution as \mathbf{F}^h .

The ResNet branch and high-res branch output feature maps are concatenated and then passed through an AVGPOOL layer. Then, we obtain the final learned representation, $\mathbf{f} \in \mathbb{R}^D$, that captures generation artifacts of the input image \mathbf{I} . Subsequently, we learn C independent linear layers, *i.e.*, $\Theta = \{\theta_{i=0}^{C-1}\}$ to transform \mathbf{f} into a set of graph node features $\mathbf{H} = \{\mathbf{h}_0, \mathbf{h}_1, \dots, \mathbf{h}_{(C-1)}\}$, where $\mathbf{H} \in \mathbb{R}^{C \times D}$ and $\mathbf{h}_i \in \mathbb{R}^{1 \times D}$ ($i \in \{0, 1, \dots, C-1\}$). We use \mathbf{H} to denote graph node features of the directed graph (*i.e.*, graph topology) $\mathbf{A} \in \mathbb{R}^{C \times C}$.

3.2.2 GCN Refinement Block

The GCN refinement block has a learnable pooling-unpooling mechanism that progressively coarsens the original graph \mathbf{A}_0 into a series of coarsened graphs, *i.e.*, $\mathbf{A}_1, \mathbf{A}_2 \dots \mathbf{A}_n$, and graph convolution is conducted on graphs at all different levels. Specifically, such a pooling operation is achieved by merging graph nodes, namely, via a learned matching matrix \mathbf{M} . Also, correlation matrices of different graphs, denoted as \mathbf{A}_l ², which are learned using MLP layers, which are also influenced by the GM responsible for generating the input image. This further emphasizes the significant impact of GM on the correlation graph generation process.

Learnable Graph Pooling Layer First, $\mathbf{A}_l \in \mathbb{R}^{m \times m}$ and $\mathbf{A}_{l+1} \in \mathbb{R}^{n \times n}$ denote directed graphs at l th and $l+1$ th layers, with m and n ($m \geq n$) graph nodes, respectively. An assignment matrix $\mathbf{M}_l \in \mathbb{R}^{m \times n}$ converts \mathbf{A}_l to \mathbf{A}_{l+1} as:

$$\mathbf{A}_{l+1} = \mathbf{M}_l^T \mathbf{A}_l \mathbf{M}_l. \quad (2)$$

Also, we use $\mathbf{H}_l \in \mathbb{R}^{m \times D}$ and $\mathbf{H}_{l+1} \in \mathbb{R}^{n \times D}$ to denote graph node features of \mathbf{A}_l and \mathbf{A}_{l+1} , respectively. Therefore, we can use \mathbf{M}_l to perform the graph node aggregation operation via:

$$\mathbf{H}_{l+1} = \mathbf{M}_l^T \mathbf{H}_l. \quad (3)$$

For simplicity, we use f_{GCN} to denote the mapping function imposed by a GCN block that has multiple GCN layers. \mathbf{H}_l^{in} and \mathbf{H}_l^{out} are the input and output feature of the l th GCN block:

$$\mathbf{H}_l^{out} = f_{GCN}(\mathbf{H}_l^{in}). \quad (4)$$

Ideally, the pooling operation and correlation between different hyperparameters should be dependent on the extracted feature of the input image. Therefore, assuming the learned feature at l th layer is \mathbf{H}_l^{out} , we employ a trainable weight, *i.e.*, \mathbf{W}_m , to transform it into the assignment matrix \mathbf{M}_l :

$$\mathbf{M}_l = \frac{1}{1 + e^{-\alpha(\mathbf{W}_m \mathbf{H}_l^{out})}} \quad (5)$$

where α is set as $1e9$. As a result, we obtain \mathbf{M}_l , in which values are exclusively set to 0 or 1.

²A l -th layer graph has nodes and connectivities (*e.g.*, correlations), and we use \mathbf{A}_l to denote the l -th layer graph or only its correlations.

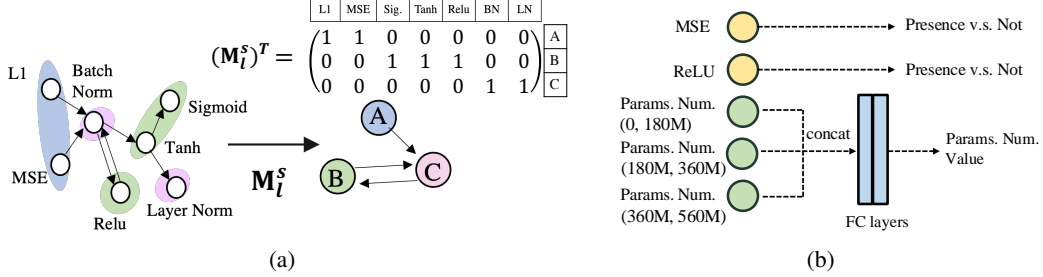


Figure 4: (a) A toy example of the hyperparameter hierarchy assignment \mathbf{M}_l^s : both L1 and L2 belong to the category of pixel-level loss function, so they are merged into the supernode A. Nonlinearity functions (e.g., ReLU and Tanh) and normalization methods (e.g., Layer Norm. and Batch Norm.) are merged into supernodes B and C, respectively. (b) In the inference, discrete-value graph node features are used to classify if discrete hyperparameters are used in the given GM. We concatenate corresponding continuous-value graph node features and regress the continuous hyperparameter value.

Learnable Unpooling Layer We perform the graph unpooling operation, which restores information to the graph at the original resolution for the original graph node classification task. As Fig. 2, to avoid confusion, we use \mathbf{H} and \mathbf{V} to represent the graph node feature on the pooling and unpooling branches, respectively. The correlation matrix on the unpooling branch is denoted by \mathbf{A}' ,

$$\mathbf{A}'_{l-1} = \mathbf{M}_l \mathbf{A}'_l \mathbf{M}_l^T; \mathbf{V}_{l-1} = \mathbf{M}_l \mathbf{V}_l, \quad (6)$$

where \mathbf{A}'_l and \mathbf{A}'_{l-1} are the l th and $l-1$ th layers in the unpooling branch. Finally, we use the refined feature \mathbf{V} for model parsing, as depicted in Fig. 2.

Discussion This learnable pooling-unpooling mechanism offers three distinct advantages. First, each supernode in the coarsened graph serves as the combination of features from its children nodes, and graph convolutions on supernodes have a large receptive field for aggregating features. Secondly, the learnable correlation models hyperparameter dependencies dynamically based on generation artifacts of input image features (e.g., \mathbf{f}). Lastly, learned correlation graphs \mathbf{A} vary across different levels, helping address the over-smoothing issue commonly encountered in GCN learning [38, 43, 5].

3.3 Training and Inference

We jointly train our method with three objective functions. Graph node classification loss (e.g., \mathcal{L}^{graph}) encourages each graph node feature to predict the corresponding hyperparameter label. Artifacts isolation loss (e.g., \mathcal{L}^{iso}) helps the LGPN only parse the hyperparameters for generated images, and hyperparameter hierarchy constraints (e.g., \mathcal{L}^{hier}) imposes hierarchical constraints among different hyperparameters while stabilizing the training.

Training Samples We denote a training sample as $\{\mathbf{I}, \mathbf{y}\}$, in which $\mathbf{y} = \{\mathbf{y}^d, \mathbf{y}^c, \mathbf{y}^l\} = \{y_0, y_1, \dots, y_{(C-1)}\}$ is its annotation for C parsed hyperparameters as introduced in Sec. 3.1. Specifically, y_c is assigned as 1 if the sample has c -th hyperparameter and 0 otherwise, where $c \in \{0, 1, \dots, C-1\}$. Details are in Supplementary Sec. B.

Graph Node Classification Loss Given the image \mathbf{I} , we convert the refined feature \mathbf{V} into the predicted score vector, denoted as $\mathbf{s} = \{s_0, s_1, \dots, s_{(C-1)}\}$. We employ the sigmoid activation to retrieve the probability vector $\mathbf{p} = \{p_0, p_1, \dots, p_{(C-1)}\}$, namely, $p_c = \text{SIGMOID}(s_c)$. Then, we have:

$$\mathcal{L}^{graph} = \sum_{c=0}^{C-1} (y_c \log p_c + (1 - y_c) \log(1 - p_c)). \quad (7)$$

Hyperparameter Hierarchy Prediction Fig. 4 shows that different hyperparameters can be grouped, so we define the hyperparameter hierarchy assignment \mathbf{M}^s to reflect this inherent nature. More details of such the assignment are in Supplementary Sec. A. Suppose, at the l th layer, we minimize the L_2 norm of the difference between the predicted matching matrix \mathbf{M}_l and \mathbf{M}_l^s ,

$$\mathcal{L}^{hier} = \|\mathbf{M}_l^s - \mathbf{M}_l\|_2 = \sqrt{\sum_{i,j=0}^{C-1} (m_{ij}^s - m_{ij})^2}. \quad (8)$$

	Method			Loss Function		Dis. Archi. Para.		Con. Archi. Para.
	ID	Backbone	MP Head	F1 ↑	Acc. ↑	F1 ↑	Acc. ↑	L1 error ↓
1	Baseline1	ResNet-50	MLP	79.0	77.7	72.1	69.0	0.163
2	Baseline2	HR-Net	MLP	80.7	81.9	72.2	70.3	0.149
3	Baseline3	ViT-B	MLP	76.3	75.9	68.3	66.4	0.177
4	Baseline4	GTC	MLP	82.5	80.9	75.7	70.9	0.135
5	FEN-PN [2]	FEN.	Parsing Net.	80.5	78.9	73.0	70.8	0.139
6	LGPN	GTC	GCN refinement	84.6	83.3	79.5	77.5	0.120

Table 1: We report model parsing performance on RED140, where each method has an individual ID that represents different backbones and model parsing (MP) heads. The comparison among different backbones () shows the effectiveness of the proposed GTC. *Loss Function* reports the averaged prediction performance on 10 loss functions. The averaged performance on 18 discrete architecture hyperparameters and 9 continuous hyperparameters are reported in *Dis. Archi. Para.* and *Con. Archi. Para.*, respectively. [**Bold**: best result].

Artifacts Isolation Loss We denote the image-level binary label as y^{img} and use p^{img} as the probability that \mathbf{I} is a generated image. Then we have:

$$\mathcal{L}^{iso} = \sum_{i=0}^{M-1} (y^{img} \log p^{img} + (1 - y^{img}) \log(1 - p^{img})). \quad (9)$$

In summary, our joint training loss function can be written as $\mathcal{L}^{all} = \lambda_1 \mathcal{L}^{graph} + \lambda_2 \mathcal{L}^{hier} + \lambda_3 \mathcal{L}^{iso}$, where λ_1 and λ_2 equal 0 when \mathbf{I} is real.

Inference As Fig. 4b, we use the discrete-value graph node feature to perform the binary classification to decide the presence of given hyperparameters. For the continuous architecture hyperparameter, we first concatenate n corresponding node feature and train a linear layer to regress it to the estimated value. Empirically, we set n as 3 and show this concatenated feature improves the robustness in predicting the continuous value (see Supplementary Tab. 7).

4 Experiment

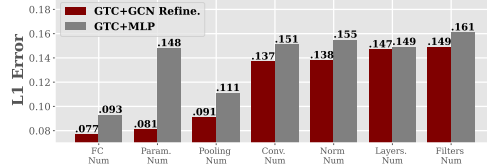
4.1 Model Parsing

Setup Our experiment utilizes RED140 dataset. In RED140, each GM contains 1,000 images, resulting in a total of 140,000 generated images that encompass a wide range of semantics, including objects, handwritten digits, and human faces. Also, RED140 has real images on which these GMs are trained, such as CelebA [40], MNIST [14], CIFAR10 [36], ImageNet [13], facades [75], edges2shoes [75] and, apple2oranges [75]. We follow the protocol of [2]: we divide samples into 4 disjoint sets, each of which comprises different GM categories such as GAN, VAE, DM, *etc.* Next, we do leave-one-out testing, *i.e.*, train on 125 GMs from three sets, and test on GMs of the remaining set. The performance is averaged across four test sets, measured by F1 score and accuracy for discrete hyperparameters (loss function and discrete architecture hyperparameters) and L1 error for continuous architecture hyperparameters. Implementation details are in Supplementary Sec. B.

Main Performance We report model parsing performance in Tab. 1, where our proposed LGPN (line #6) largely outperforms previous model parsing algorithms. We first employ commonly used backbones to set up competitive model parsing baselines for a more comprehensive comparison. More formally, four baselines in lines #1—4 that use ResNet-50, ViT-B, HR-Net, and GTC as backbones with 2 layers MLP as the model parsing head, respectively. Baseline4 (line #4) achieves the best performance, which indicates that GTC is the most suitable backbone for model parsing. Specifically, Baseline4 has 1.8% and 3.5% higher F1 score over Baseline2 that uses HR-Net on predicting hyperparameters of loss functions and discrete architecture hyperparameters. After that, we report FEN-PN’s performance, which already proves the effectiveness on the model parsing task since it has specific model parsing architectures containing a fingerprint estimate network (FEN) and a parsing network that predicts hyperparameters. Surprisingly, although FEN-PN has achieved competitive results on RED116, it only has comparable performance to Baseline2. This indicates that FEN-PN reduces its effectiveness in predicting hyperparameters of diffusion models, as RED140

	Method		Loss Function		Dis. Archi. Para.	
	Backbone	MP Head	F1 \uparrow	Acc. \uparrow	F1 \uparrow	Acc. \uparrow
1	GTC	MLP	82.5	80.9	75.7	70.9
2		Stacked GCN	83.2	81.3	76.9	73.8
3		Att-GCN [59]	83.4	82.7	78.0	74.5
4		Graph U-Net [19]	82.2	82.0	74.8	70.2
5		GCN refinement	84.6	83.3	79.5	77.5

(a)



(b)

Table 2: (a) Model parsing performance comparison with different GCN variants. (b) The GCN refinement block improves prediction performance on continuous hyperparameters.

	Training Objectives			F1 score \uparrow	
	L_{graph}	L_{iso}	L_{hier}	Loss Fun.	Dis. Archi. Para.
✓	✓			83.7	77.0
✓		✓		84.0	78.1
✓			✓	83.9	79.0
✓	✓	✓	✓	84.6	79.5

(a)

(b)

Method	Loss Function	Dis. Archi. Para.	Con. Archi. Para.
	F1 score \uparrow	F1 score \uparrow	L1 error \downarrow
FEN-PN [2]	81.3	71.8	0.149
GTC w MLP	77.8	68.9	0.169
GTC w S-GCN	79.0	69.8	0.145
LGPN	84.1	74.3	0.130

(c)

Figure 5: a) Cosine similarity between generated correlation graphs (*i.e.*, A'_0) for *unseen* GMs in one of four test sets. Each element of this matrix is the average cosine similarities of 2,000 pairs of generated correlation graphs A'_0 from corresponding GMs. b) The ablation on three objective functions, defined in Sec. 3.3. c) The model parsing performance on RED116 dataset. [Key: **Best**; S-GCN: stacked GCN]

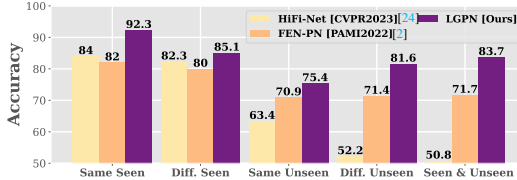
contains more images from diffusion models than RED116. The complete performance comparison on RED116 is reported in Tab. 5c. Lastly, we replace MLP with the GCN refinement block, which is the full model of LGPN (line #6) and performs better on all metrics, demonstrating that the GCN refinement block indeed refines graph node features and makes a more effective model parsing head than MLP layers.

Hyperparameter Dependency Capturing Tab. 2a reports model parsing performance using different GCN variants as the model parsing head. Overall, the proposed GCN refinement block, which refines graph node features to better capture hyperparameter dependencies, helps achieve the best model parsing performance. By comparing lines #1 and #2, we conclude that replacing MLP layers with the GCN refinement benefits the model parsing task. After all, GCN leverages structural information of the pre-defined graph, improving the learning of correlations among different hyperparameters. Next, we use *Graph attention networks* [59] (Att-GCN) at line #3, which employs the attention mechanism to update the graph node feature. As a result, Att-GCN achieves 1.1% higher F1 than stacked GCN (*e.g.*, line #2) on predicting discrete architecture parameters. Lastly, line #4 uses *Graph U-Net* [19], which has a similar pooling-unpooling mechanism to our GCN refinement block, but its pooling operation discards graph nodes in the previous layer for forming a smaller graph. Using the Graph U-Net as the model parsing head produces the worse performance on discrete architecture hyperparameters — 4.3% lower than Att-GCN (#3). We believe this is because dropping graph nodes is not optimal for model parsing, in which all graph nodes represent corresponding hyperparameters and are important for the final performance. In contrast, LGPN merges children nodes into the supernode, so all node information in the previous layer remains in the smaller pooled graph, helping achieve the best performance on discrete hyperparameters in Tab. 2a. On the other hand, *continuous hyperparameter prediction* can also benefit from the GCN refinement block. In Tab. 2b, LGPN shows L1 errors of 0.147 and 0.081 on Layers Num. and Param. Num. respectively, whereas the model with MLP layers only achieves 0.149 and 0.148, respectively. This is because the GCN refinement learns the dependency between Param. Num. and Layer Num., which aligns with the observation that models with more layers typically have more parameters. Therefore, modeling such dependencies ultimately decreases the L1 error in Param. Num. prediction. Likewise, when predicting Conv. Layer Num. and Filters Num., the GCN refinement achieves 0.137 and 0.149 L1 error, whereas GTC with MLP layers have 0.151 and 0.161 L1 error.

GM-dependent Graph Fig. 5a shows that learned correlation graphs (A'_0) from image pairs exhibit significant similarity when both images belong to the same *unseen* GM. This result demonstrates that our correlation graph largely depends on the GM instead of image contents, given that we have

Method	Acc.	AUC	Pd@5%
HiFi-Net [24]	72.3	75.4	30.4
FEN-PN [2]	83.0	92.4	61.2
GTC w MLP	83.9	92.2	62.5
GTC w S-GCN	84.3	94.2	68.6
LGPN	85.9	95.7	77.2

(a)



(b)

Table 3: (a) The average coordinate attack detection performance on 4-fold cross validation. (b) Test image pairs in coordinate attack detection are from one of 5 cases, bar charts from left to right: same and different GMs in seen set; same or different GMs in unseen set; one GM is from seen set and the other from unseen set. [Key: S-GCN: stacked GCN]

different contents (*e.g.*, human face and objects) in unseen GMs from each test. In addition, we empirically observe our method remains robust when using different thresholds to construct the graph, which is detailed in the Supplementary Tab. 9. However, the performance declines more when the threshold increases to 0.65, which causes the correlation graph to have very sparse connectivities, hindering the learning of hyperparameter dependencies.

Objective Functions Analysis Fig. 5b shows the ablation of different training objective functions introduced in Sec. 3.3. Line #1 only optimizes the LGPN with \mathcal{L}^{grpah} , producing results comparable to simply stacking GCN with the attention mechanism (*e.g.*, line #3 in Tab. 2a). Lines #2 and #3 show contributions from \mathcal{L}^{iso} and \mathcal{L}^{hier} , which improve the performance by 1.1% and 2.0% than only using \mathcal{L}^{grpah} , on predicting discrete architecture hyperparameters, respectively. This is because \mathcal{L}^{iso} and \mathcal{L}^{hier} make the LGPN concentrate on learning generation traces from generated images and impose the hierarchical constraints, respectively.

RED116 Results Fig. 5c reports that LGPN achieves the best performance on all metrics in RED116 dataset. Interestingly, LGPN obtains 79.5% F1 score on predicting discrete architecture hyperparameters in RED140 (Tab. 1), whereas only 74.3% in RED116, which does not contain diffusion model generated images. We believe this is because all diffusion models share similar architectures, and such similarities make the prediction of their architecture hyperparameters easier.

4.2 Coordinate Attack Detection

We evaluate the proposed LGPN on coordinated attacks detection [2], which aims to classify whether two fake images are generated from the same GM or not. This is achieved by computing the cosine similarity between predicted hyperparameters from given images. Specifically, we evaluate coordinated attack detection on RED140 in a 4-fold cross-validation. In each fold, the train set has 125 GMs, and the test set has 30 GMs where 15 GMs are exclusive (unseen) from the train set and 15 GMs are seen in the train set. We generate 89,000 training image pairs from train-set GMs for training 1,000 image pairs for validation. We generate 25,000 test image pairs from test-set GMs, and the average of the 4 folds is used as the final result. For the measurement, we use accuracy, AUC, and detection probability at a fixed false alarm rate (Pd@FAR) *e.g.*, Pd@5% as metrics. Specifically, aside from FEN-PN [2], we also compare with the recent work HiFi-Net [24] that show SoTA results in attributing different forgery methods. Specifically, we train HiFi-Net to classify 125 GMs and take learned features from the last fully-connected layer for coordinated attack detection. The performance is reported in Tab. 3a, which demonstrates that our proposed method surpasses both prior works. We observe the HiFi-Net performs much worse on AUC than the model parsing baseline (*e.g.*, GTC w S-GCN) and FEN-PN. Furthermore, Tab. 3b shows the FEN-PN and LGPN perform comparably as HiFi-Net on seen GMs (first two bar charts), yet much better than HiFi-Net when images are generated by unseen GMs (last three bar charts). Lastly, LGPN has a better Pd@5% performance than other methods.

4.3 Capturing Generation Traces

To study GTC’s ability to identify generation traces, we adopt it for CNN-generated image detection and image attribution. For a fair comparison, *no* model parsing dataset is used for the pre-training.

CNN-generated Image Detection We append fully-connected layers at the end of GTC to obtain a binary detector that distinguishes CNN-generated images from real ones (detailed in supplementary

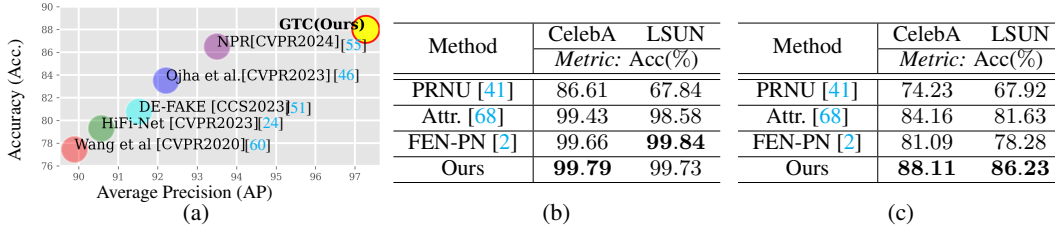


Figure 6: (a) CNN-generated image detection performance. (b) and (c) report image attribution performance in two different protocols.

Fig. 8). We follow the experiment setup from prior works [60, 46, 55], which trains the model on images generated by ProGAN [32], and test it on images generated by 11 unseen forgery methods, using average precision (AP) and accuracy for the measurement. Fig. 6a reports that our method achieves premium detection performance compared to prior methods. The second-best method, NPR [55], focuses on learning local up-sampling artifacts from pixels, helping detect images from unseen GMs. Instead, GTC’s high-resolution representation more effectively exploits both local and global traces left from generation processes, obtaining a better performance.

Image Attribution Tab. 6b and Tab. 6c report the image attribution performance in two different protocols. Specifically, we define the protocol 1 based on the previous work [2], which trains methods on 100,000 real and 100,000 images generated from four different GMs (*e.g.*, SNGAN, MMDGAN, CRAMERGAN, and ProGAN), conducting a five-way classification (*i.e.*, 4 GMs and real). In protocol 2, we add two more generative methods (*e.g.*, styleGANv2, styleGANv3), resulting in a more challenging task: a 7-way classification task, classifying whether the image is real samples or generated by which one of 6 GMs. As depicted in Supplementary Fig. 8, we apply fully-connected layers on the top of GTC, which leverages the final representation of the generation trace for the multi-category classification task, *e.g.*, image attribution. Our proposed method achieves the best image attribution performance on CelebA and competitive results on LSUN, indicating that GTC has a promising ability to capture the generation trace.

5 Conclusion

In this study, our focus is *model parsing*, which predicts pre-defined hyperparameters of a GM given an input image. We propose a novel method that incorporates a learnable pooling-unpooling mechanism devised for the model parsing task. This mechanism serves multiple purposes: modeling GM-dependent hyperparameter dependencies, expanding the receptive field of graph convolution, and mitigating the over-smoothing issue in GCN learning. In addition, we provide the Generation Trace Capturing network to capture generation artifacts, which proves effective in two different image forensic applications: CNN-generated image detection and coordinated attacks detection.

Limitation We empirically observe two limitations in our proposed method, both of which can be interesting directions for future research. First, while our model parsing approach delivers excellent performance on the RED140 dataset, it is worth exploring its effectiveness on specific GMs that fall outside our dataset scope. This investigation would provide valuable insights into the generalizability of our method to a broader range of GMs. Secondly, we formulate the model parsing task as a closed-set classification problem, which limits its ability to predict undefined hyperparameters, *e.g.*, LeakyReLU. One interesting solution could be adding a few new graph nodes for undefined hyperparameters while keeping original graph nodes — the learned dependency between graph nodes representing ReLU and LeakyReLU should be high.

Broader Impact We strongly advocate for the machine learning and computer vision community to actively work towards mitigating potential negative societal implications of research. It is possible that generated face images used in training could leak the identity information of subjects who have not provided consent forms. We shall strive to work on real face imagery whose collection is reviewed by an Institutional Review Board (IRB).

Acknowledge This work was supported by the Defense Advanced Research Projects Agency (DARPA) under Agreement No. HR00112090131 to Xiaoming Liu at Michigan State University.

References

- [1] Vishal Asnani, Xi Yin, Tal Hassner, and Xiaoming Liu. Malp: Manipulation localization using a proactive scheme. In *CVPR*, 2023.
- [2] Vishal Asnani, Xi Yin, Tal Hassner, and Xiaoming Liu. Reverse engineering of generative models: Inferring model hyperparameters from generated images. *PAMI*, 2023.
- [3] Lejla Batina, Shivam Bhasin, Dirmanto Jap, and Stjepan Picek. CSI NN: Reverse engineering of neural network architectures through electromagnetic side channel. In *USENIXSS*, 2019.
- [4] Lucy Chai, David Bau, Ser-Nam Lim, and Phillip Isola. What makes fake images detectable? understanding properties that generalize. In *ECCV*, 2020.
- [5] Deli Chen, Yankai Lin, Wei Li, Peng Li, Jie Zhou, and Xu Sun. Measuring and relieving the over-smoothing problem for graph neural networks from the topological view. In *AAAI*, 2020.
- [6] Liang Chen, Yong Zhang, Yibing Song, Lingqiao Liu, and Jue Wang. Self-supervised learning of adversarial example: Towards good generalizations for deepfake detection. In *CVPR*, 2022.
- [7] Tianshui Chen, Muxin Xu, Xiaolu Hui, Hefeng Wu, and Liang Lin. Learning semantic-specific graph representation for multi-label image recognition. In *ICCV*, 2019.
- [8] Ying Chen, Shixiong Xia, Jiaqi Zhao, Yong Zhou, Qiang Niu, Rui Yao, Dongjun Zhu, and Dongjingdian Liu. Rest-reid: Transformer block-based residual learning for person re-identification. *Pattern Recognition Letters*, 2022.
- [9] Yunpeng Chen, Marcus Rohrbach, Zhicheng Yan, Yan Shuicheng, Jiashi Feng, and Yannis Kalantidis. Graph-based global reasoning networks. In *CVPR*, 2019.
- [10] Zhao-Min Chen, Xiu-Shen Wei, Peng Wang, and Yanwen Guo. Multi-label image recognition with graph convolutional networks. In *CVPR*, 2019.
- [11] Yunjey Choi, Minje Choi, Munyoung Kim, Jung-Woo Ha, Sunghun Kim, and Jaegul Choo. StarGAN: Unified generative adversarial networks for multi-domain image-to-image translation. In *CVPR*, 2018.
- [12] Riccardo Corvi, Davide Cozzolino, Giada Zingarini, Giovanni Poggi, Koki Nagano, and Luisa Verdoliva. On the detection of synthetic images generated by diffusion models. In *ICASSP*, 2023.
- [13] Jia Deng, Wei Dong, Richard Socher, Li-Jia Li, Kai Li, and Li Fei-Fei. Imagenet: A large-scale hierarchical image database. In *CVPR*, 2009.
- [14] Li Deng. The mnist database of handwritten digit images for machine learning research. *IEEE signal processing magazine*, 2012.
- [15] Prafulla Dhariwal and Alexander Nichol. Diffusion Models Beat GANs on Image Synthesis. In *NeurIPS*, 2021.
- [16] Henghui Ding, Hui Zhang, Jun Liu, Jiabin Li, Zijian Feng, and Xudong Jiang. Interaction via bi-directional graph of semantic region affinity for scene parsing. In *ICCV*, 2021.
- [17] Emilien Dupont, Yee Whye Teh, and Arnaud Doucet. Generative models as distributions of functions. In *AISTATS*, 2021.
- [18] Wenqi Fan, Yao Ma, Qing Li, Yuan He, Eric Zhao, Jiliang Tang, and Dawei Yin. Graph neural networks for social recommendation. In *WWW*, 2019.
- [19] Hongyang Gao and Shuiwang Ji. Graph u-nets. In *ICML*, 2019.
- [20] Candice R Gerstner and Hany Farid. Detecting real-time deep-fake videos using active illumination. In *CVPR*, 2022.
- [21] Yifan Gong, Yuguang Yao, Yize Li, Yimeng Zhang, Xiaoming Liu, Xue Lin, and Sijia Liu. Reverse engineering of imperceptible adversarial image perturbations. In *ICLR*, 2022.
- [22] Ian Goodfellow, Jean Pouget-Abadie, Mehdi Mirza, Bing Xu, David Warde-Farley, Sherjil Ozair, Aaron Courville, and Yoshua Bengio. Generative adversarial nets. In *NeurIPS*, 2014.
- [23] Xiao Guo, Xiaohong Liu, Iacopo Masi, and Xiaoming Liu. Language-guided hierarchical fine-grained image forgery detection and localization. *IJCV*, 2024.

- [24] Xiao Guo, Xiaohong Liu, Zhiyuan Ren, Steven Grosz, Iacopo Masi, and Xiaoming Liu. Hierarchical fine-grained image forgery detection and localization. In *CVPR*, 2023.
- [25] Xiao Guo, Yaojie Liu, Anil Jain, and Xiaoming Liu. Multi-domain learning for updating face anti-spoofing models. In *ECCV*, 2022.
- [26] Zhijiang Guo, Yan Zhang, and Wei Lu. Attention guided graph convolutional networks for relation extraction. In *ACL*, 2019.
- [27] Jonathan Ho, Ajay Jain, and Pieter Abbeel. Denoising diffusion probabilistic models. In *NeurIPS*, 2020.
- [28] I Hsu, Xiao Guo, Premkumar Natarajan, and Nanyun Peng. Discourse-level relation extraction via graph pooling. In *AAAI DLG workshop*, 2021.
- [29] Hanzhe Hu, Deyi Ji, Weihao Gan, Shuai Bai, Wei Wu, and Junjie Yan. Class-wise dynamic graph convolution for semantic segmentation. In *ECCV*, 2020.
- [30] Weizhe Hua, Zhiru Zhang, and G Edward Suh. Reverse engineering convolutional neural networks through side-channel information leaks. In *DAC*, 2018.
- [31] Kaixiang Ji, Feng Chen, Xin Guo, Yadong Xu, Jian Wang, and Jingdong Chen. Uncertainty-guided learning for improving image manipulation detection. In *ICCV*, 2023.
- [32] Tero Karras, Timo Aila, Samuli Laine, and Jaakko Lehtinen. Progressive growing of gans for improved quality, stability, and variation. In *ICLR*, 2018.
- [33] Tero Karras, Samuli Laine, and Timo Aila. A style-based generator architecture for generative adversarial networks. In *CVPR*, 2019.
- [34] Gwanghyun Kim, Taesung Kwon, and Jong Chul Ye. DiffusionCLIP: Text-guided diffusion models for robust image manipulation. In *CVPR*, 2022.
- [35] Thomas N Kipf and Max Welling. Semi-supervised classification with graph convolutional networks. In *ICLR*, 2017.
- [36] Alex Krizhevsky and Geoffrey Hinton. Learning multiple layers of features from tiny images. Technical report, 2009.
- [37] Yann LeCun, Léon Bottou, Yoshua Bengio, and Patrick Haffner. Gradient-based learning applied to document recognition. *Proceedings of the IEEE*, 1998.
- [38] Guohao Li, Matthias Muller, Ali Thabet, and Bernard Ghanem. Deepgens: Can gcons go as deep as cnns? In *ICCV*, 2019.
- [39] Xia Li, Yibo Yang, Qijie Zhao, Tiancheng Shen, Zhouchen Lin, and Hong Liu. Spatial pyramid based graph reasoning for semantic segmentation. In *CVPR*, 2020.
- [40] Ziwei Liu, Ping Luo, Xiaogang Wang, and Xiaoou Tang. Deep learning face attributes in the wild. In *ICCV*, 2015.
- [41] Francesco Marra, Diego Gragnaniello, Luisa Verdoliva, and Giovanni Poggi. Do GANs leave artificial fingerprints? In *MIPR*, 2019.
- [42] Safa C. Medin, Bernhard Egger, Anoop Cherian, Ye Wang, Joshua B. Tenenbaum, Xiaoming Liu, and Tim K. Marks. MOST-GAN: 3D morphable StyleGAN for disentangled face image manipulation. In *AAAI*, 2022.
- [43] Yimeng Min, Frederik Wenkel, and Guy Wolf. Scattering GCN: Overcoming oversmoothness in graph convolutional networks. In *NeurIPS*, 2020.
- [44] Binh X Nguyen, Binh D Nguyen, Tuong Do, Erman Tjiputra, Quang D Tran, and Anh Nguyen. Graph-based person signature for person re-identifications. In *CVPR*, 2021.
- [45] Seong Joon Oh, Bernt Schiele, and Mario Fritz. Towards reverse-engineering black-box neural networks. *Explainable AI: interpreting, explaining and visualizing deep learning*, pages 121–144, 2019.
- [46] Utkarsh Ojha, Yuheng Li, and Yong Jae Lee. Towards universal fake image detectors that generalize across generative models. In *CVPR*, 2023.

- [47] Yongyang Pan, Xiaohong Liu, Siqi Luo, Yi Xin, Xiao Guo, Xiaoming Liu, Xionghuo Min, and Guangtao Zhai. Towards effective user attribution for latent diffusion models via watermark-informed blending. *arXiv preprint arXiv:2409.10958*, 2024.
- [48] Robin Rombach, Andreas Blattmann, Dominik Lorenz, Patrick Esser, and Björn Ommer. High-resolution image synthesis with latent diffusion models. In *CVPR*, 2022.
- [49] Michael Schlichtkrull, Thomas N Kipf, Peter Bloem, Rianne Van Den Berg, Ivan Titov, and Max Welling. Modeling relational data with graph convolutional networks. In *ESWC*, 2018.
- [50] Husrev Taha Sencar, Luisa Verdoliva, and Nasir Memon. *Multimedia Forensics*. Springer Nature, 2022.
- [51] Zeyang Sha, Zheng Li, Ning Yu, and Yang Zhang. De-fake: Detection and attribution of fake images generated by text-to-image generation models. In *Proceedings of the 2023 ACM SIGSAC Conference on Computer and Communications Security*, pages 3418–3432, 2023.
- [52] Kaede Shiohara and Toshihiko Yamasaki. Detecting deepfakes with self-blended images. In *CVPR*, 2022.
- [53] Xiufeng Song, Xiao Guo, Jiache Zhang, Qirui Li, Lei Bai, Xiaoming Liu, Guangtao Zhai, and Xiaohong Liu. On learning multi-modal forgery representation for diffusion generated video detection. In *NeurIPS*, 2024.
- [54] Zhihao Sun, Haoran Jiang, Danding Wang, Xirong Li, and Juan Cao. Safl-net: Semantic-agnostic feature learning network with auxiliary plugins for image manipulation detection. In *ICCV*, 2023.
- [55] Chuangchuang Tan, Huan Liu, Yao Zhao, Shikui Wei, Guanghua Gu, Ping Liu, and Yunchao Wei. Rethinking the up-sampling operations in cnn-based generative network for generalizable deepfake detection. In *CVPR*, 2024.
- [56] Praveen Tirupattur, Kevin Duarte, Yogesh S Rawat, and Mubarak Shah. Modeling multi-label action dependencies for temporal action localization. In *CVPR*, 2021.
- [57] Florian Tramèr, Fan Zhang, Ari Juels, Michael K Reiter, and Thomas Ristenpart. Stealing machine learning models via prediction APIs. In *USENIXSS*, 2016.
- [58] Luan Tran, Xi Yin, and Xiaoming Liu. Disentangled representation learning GAN for pose-invariant face recognition. In *CVPR*, 2017.
- [59] Petar Veličković, Guillem Cucurull, Arantxa Casanova, Adriana Romero, Pietro Lio, and Yoshua Bengio. Graph attention networks. In *ICLR*, 2017.
- [60] Sheng-Yu Wang, Oliver Wang, Richard Zhang, Andrew Owens, and Alexei A Efros. Cnn-generated images are surprisingly easy to spot... for now. In *CVPR*, 2020.
- [61] Zhendong Wang, Jianmin Bao, Wengang Zhou, Weilun Wang, Hezhen Hu, Hong Chen, and Houqiang Li. Dire for diffusion-generated image detection. In *ICCV*, 2023.
- [62] Yue Wu, Wael AbdAlmageed, and Premkumar Natarajan. Mantra-net: Manipulation tracing network for detection and localization of image forgeries with anomalous features. In *CVPR*, 2019.
- [63] Yingmao Yao, Xiaoyan Jiang, Hamido Fujita, and Zhijun Fang. A sparse graph wavelet convolution neural network for video-based person re-identification. *Pattern Recognition*, 2022.
- [64] Yuguang Yao, Xiao Guo, Vishal Asnani, Yifan Gong, Jiancheng Liu, Xue Lin, Xiaoming Liu, Sijia Liu, et al. Reverse engineering of deceptions on machine-and human-centric attacks. *Foundations and Trends® in Privacy and Security*, 6(2):53–152, 2024.
- [65] Yuguang Yao, Jiancheng Liu, Yifan Gong, Xiaoming Liu, Yanzhi Wang, Xue Lin, and Sijia Liu. Can adversarial examples be parsed to reveal victim model information? In *WACV*, 2024.
- [66] Jin Ye, Junjun He, Xiaojiang Peng, Wenhao Wu, and Yu Qiao. Attention-driven dynamic graph convolutional network for multi-label image recognition. In *ECCV*, 2020.
- [67] Fisher Yu, Ari Seff, Yinda Zhang, Shuran Song, Thomas Funkhouser, and Jianxiong Xiao. LSUN: Construction of a large-scale image dataset using deep learning with humans in the loop. *arXiv preprint arXiv:1506.03365*, 2015.
- [68] Ning Yu, Larry S Davis, and Mario Fritz. Attributing fake images to GANs: Learning and analyzing GAN fingerprints. In *ICCV*, 2019.

- [69] Yuanhao Zhai, Tianyu Luan, David Doermann, and Junsong Yuan. Towards generic image manipulation detection with weakly-supervised self-consistency learning. In *ICCV*, 2023.
- [70] Lingzhi Zhang, Zhengjie Xu, Connelly Barnes, Yuqian Zhou, Qing Liu, He Zhang, Sohrab Amirghodsi, Zhe Lin, Eli Shechtman, and Jianbo Shi. Perceptual artifacts localization for image synthesis tasks. In *ICCV*, 2023.
- [71] Lvmin Zhang, Anyi Rao, and Maneesh Agrawala. Adding conditional control to text-to-image diffusion models. In *ICCV*, 2023.
- [72] Xu Zhang, Svebor Karaman, and Shih-Fu Chang. Detecting and simulating artifacts in gan fake images. In *WIFS*, 2019.
- [73] Yue Zhang, Ben Colman, Ali Shahriyari, and Gaurav Bharaj. Common sense reasoning for deep fake detection. *arXiv preprint arXiv:2402.00126*, 2024.
- [74] Jizhe Zhou, Xiaochen Ma, Xia Du, Ahmed Y Alhammedi, and Wentao Feng. Pre-training-free image manipulation localization through non-mutually exclusive contrastive learning. In *ICCV*, 2023.
- [75] Jun-Yan Zhu, Taesung Park, Phillip Isola, and Alexei A Efros. Unpaired image-to-image translation using cycle-consistent adversarial networks. In *ICCV*, 2017.

In this supplementary, we provide:

- ◊ Predictable hyperparameters introduction.
- ◊ Training and implementation details.
- ◊ Additional results of model parsing and CNN-generated image detection.
- ◊ The construction of RED140 dataset.
- ◊ Hyperparameter ground truth and the model parsing performance for each GM

A Predictable Hyperparameters Introduction

We investigate 37 hyperparameters that exhibit the predictability according to Asnani *et al.* [2]. These hyperparameters are categorized into three groups: (1) Loss Function (Tab. 4), (2) Discrete Architecture Hyperparameters (Tab. 5), (3) Continuous Architecture Hyperparameters (Tab. 6). We report our proposed method performance of parsing hyperparameters in these three groups via Fig. 7a, Fig. 7b, and Fig. 7c, respectively. Moreover, in the main paper’s Eq. 8 and Fig. 4a, we employ the assignment hierarchy M^s to group different hyperparameters together, which supervises the learning of the matching matrix M . The construction of such the M^s is also based on Tab. 4, 5, and 6, which not only define three coarse-level categories, but also fine-grained categories such as pixel-level objective (loss) function (*e.g.*, L1 and MSE) in Tab. 4, and normalization methods (*e.g.*, ReLU and Tanh) as well as nonlinearity functions (*e.g.*, Layer Norm. and Batch Norm.) in Tab. 5.

B Training and Implementation Details

Training Details Given the directed graph $A \in \mathbb{R}^{C \times C}$, which contains C graph nodes. We empirically set C as 55, as mentioned in the main paper Sec. 3.3. In the training, LGPN takes the given image I and output the refined feature $V \in \mathbb{R}^{55 \times D}$, which contains learned features for each graph node, namely, $V = \{v_0, v_1, \dots, v_{54}\}$. As a matter of fact, we can view V as three separate sections: $V^l = \{v_0, v_1, \dots, v_9\}$, $V^d = \{v_{10}, v_{11}, \dots, v_{27}\}$, and $V^c = \{v_{28}, v_{29}, \dots, v_{54}\}$, which denote learned features for graph nodes of 10 loss functions (*e.g.*, L1 and MSE), 18 discrete architecture hyperparameter (*e.g.*, Batch Norm. and ReLU), and 9 continuous architecture hyperparameter (*i.e.*, Parameter Num.), respectively. Note V^c represents learned features of 9 continuous architecture hyperparameters because each continuous hyperparameter is represented by 3 graph nodes, as illustrated in Fig. 1c of the main paper. Furthermore, via Eq. 7 in the main paper, we use V to obtain the corresponding probability score $p = \{p_0, p_1, \dots, p_{54}\}$ for each graph node. Similar to V , this p can be viewed as three sections: $p^l \in \mathbb{R}^{10}$, $p^d \in \mathbb{R}^{18}$ and $p^c \in \mathbb{R}^{27}$ for loss functions, discrete architecture hyperparameters, continuous architecture hyperparameters, respectively. In the end, we use p to help optimize LGPN via the graph node classification loss (Eq. 7). After the training converges, we further apply individual fully connected layers on the top of frozen learned features of continuous architecture hyperparameters (*e.g.*, V^c). via minimizing the \mathcal{L}_1 distance between predicted and ground truth value.

In the inference (the main paper Fig. 4b), for loss function and discrete architecture hyperparameters, we use output probabilities (*e.g.*, p^l and p^d) of discrete value graph nodes, for the binary “used v.s. not” classification. For the continuous architecture hyperparameters, we first concatenate learned features of corresponding graph nodes. We utilize such a concatenated feature with pre-trained, fully connected layers to estimate the continuous hyperparameter value.

Model Parsing Implementation Details Denote the output feature from the Generation Trace Capturing Network as $f \in \mathbb{R}^{2048}$. To transform f into a set of features $H = \{h_0, h_1, \dots, h_{54}\}$ for the 55 graph nodes, 55 independent linear layers (Θ) are employed. Each feature h_i is of dimension \mathbb{R}^{512} . The H is fed to the GCN refinement block, which contains 5 GCN blocks, each of which has 2 stacked GCN layers. In other words, the GCN refinement block has 10 layers in total. We use the correlation graph $A \in \mathbb{R}^{55 \times 55}$ (Fig. 10) to capture the hyperparameter dependency and during the training the LGPN pools A into $A_1 \in \mathbb{R}^{18 \times 18}$ and $A_2 \in \mathbb{R}^{6 \times 6}$ as the Fig. 2 of the main paper. The LGPN is implemented using the PyTorch framework. During training, a learning rate of $3e-2$ is used. The training is performed with a batch size of 400, where 200 images are generated by various GMs and 200 images are real.

Table 4: Loss Function types used by all GMs. We group the 10 loss functions into three categories. We use the binary representation to indicate the presence of each loss type in training the respective GM.

Category	Loss Function
Pixel-level	L_1
	L_2
	Mean squared error (MSE)
	Maximum mean discrepancy (MMD)
Discriminator	Least squares (LS)
	Wasserstein loss for GAN (WGAN)
	Kullback–Leibler (KL) divergence
	Adversarial
Classification	Hinge
	Cross-entropy (CE)

Table 5: Discrete Architecture Hyperparameters used by all GMs. We group the 18 discrete architecture hyperparameters into 6 categories. We use the binary representation to indicate the presence of each hyperparameter type in training the respective GM.

Category	Discrete Architecture Hyperparameters
Normalization	Batch Normalization
	Instance Normalization
	Adaptive Instance Normalization
	Group Normalization
Nonlinearity in the Last Layer	ReLU
	Tanh
	Leaky_ReLU
	Sigmoid
	SiLU
Nonlinearity in the Last Block	ELU
	ReLU
	Leaky_ReLU
	Sigmoid
	SiLU
Up-sampling	Nearest Neighbour Up-sampling
Skip Connection	Deconvolution
Down-sampling	Feature used
	Feature used

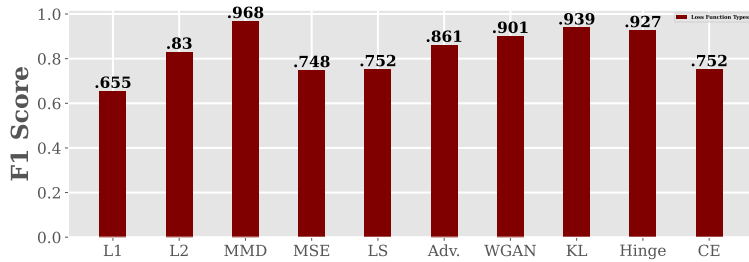
Table 6: Continuous Architecture Hyperparameters used by all GMs, where "[" denotes inclusive and ")" denotes exclusive intervals. We report the range for 9 continuous hyperparameters.

Category	Range	Discrete Architecture Hyperparameters
Layer Number	(0—717]	Layers Number
	[0—289]	Convolution Layer Number
	[0—185]	Fully-connected Layer Number
	[0—46]	Pooling Layer Number
	[0—235]	Normalization Layer Number
	(0—20]	Layer Number per Block
Unit Number	(0—8, 365]	Filter Number
	(0—155]	Block Number
	(0—56, 008, 488]	Parameter Number

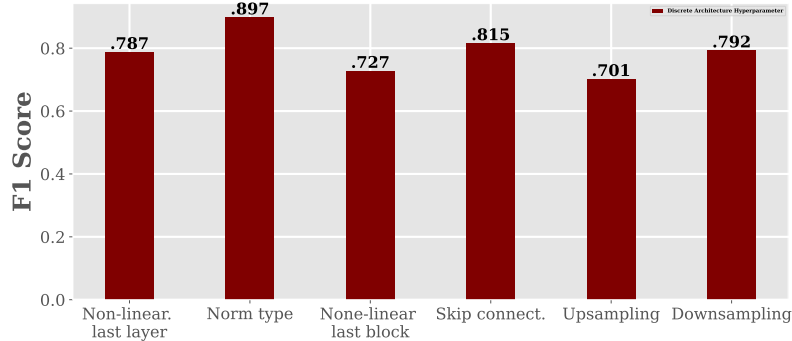
Implementation Details for Detection and Attributions We validate GTC’s effectiveness in capturing the generation trace in Fig. 6. Specifically, Fig. 8 shows the detailed implementation. We employ FC layers to convert output feature $\mathbf{f} \in \mathbb{R}^{2048}$ to $\mathbf{f}_{det.} \in \mathbb{R}^2$ and $\mathbf{f}_{att.} \in \mathbb{R}^5$ for CNN-generated image detection and image attribution respectively.

C Additional Results

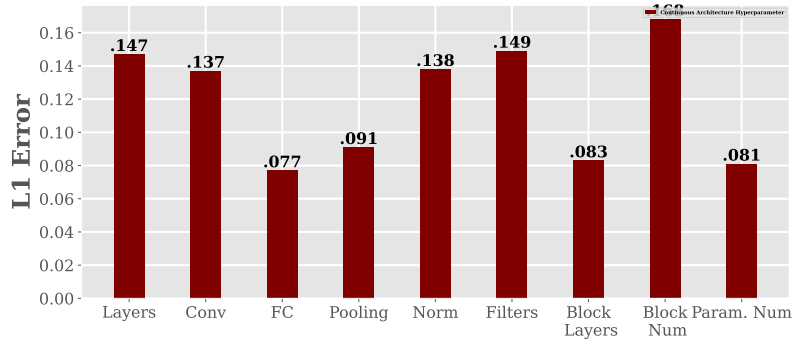
We report detailed performance on RED116 via Tab. 8, demonstrating that our proposed LGPN achieves the best performance on both datasets. Also, in Fig. 5a of the main paper, we visualize



(a)



(b)



(c)

Figure 7: (a) The F1 score on the loss function reveals that MMD and KL are two easiest loss functions to predict. (b) The F1 score on the discrete architecture hyperparameters demonstrates that predicting these hyperparameters is more challenging than predicting the loss function. This finding aligns with the empirical results reported in the previous work [2]. (c) The L1 error on the continuous architecture hyperparameters indicates that it is challenging to predict Block Num. and Filter Num..

n Value	2	3	4	5	6
L1 Error	0.123	0.120	0.124	0.132	0.130

Table 7: Using different n graph nodes for the continuous hyperparameter regression.

the correlation graph similarities among different GMs in the first test set. In this section, we offer a similar visualization (*e.g.*, Fig. 9 of the supplementary) for other test sets. In the main paper’s Sec 3.3, we use n graph nodes for each continuous hyperparameter and n is set as 3. Tab. 7 shows the advantage of choice, which shows the lowest \mathcal{L}_1 regression error is achieved when n is 3.



Figure 8: We construct simple classifiers based on GTC. Then, we train these two classifiers for CNN-generated image detection and image attribution, respectively. Please note that GTC only leverages ImageNet pre-trained weights as the initialization, same as the previous method [60]. For a fair comparison, no model parsing datasets such as RED116 and RED140 are used for pre-training.

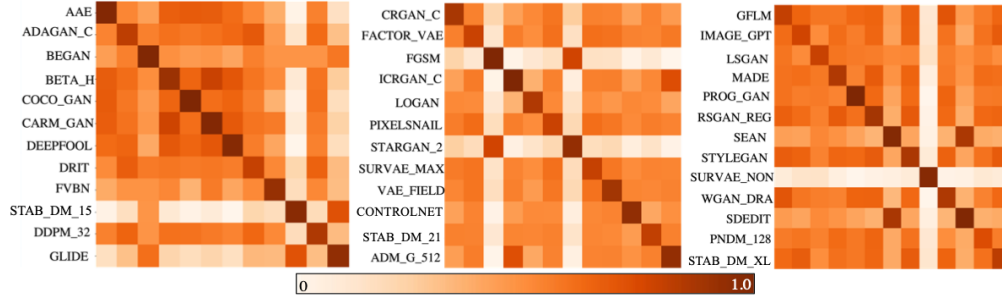


Figure 9: Each element of these two matrices is the average cosine similarities of 2,000 pairs of generated correlation graphs A'_0 from corresponding GMs in the second, third and fourth test sets.

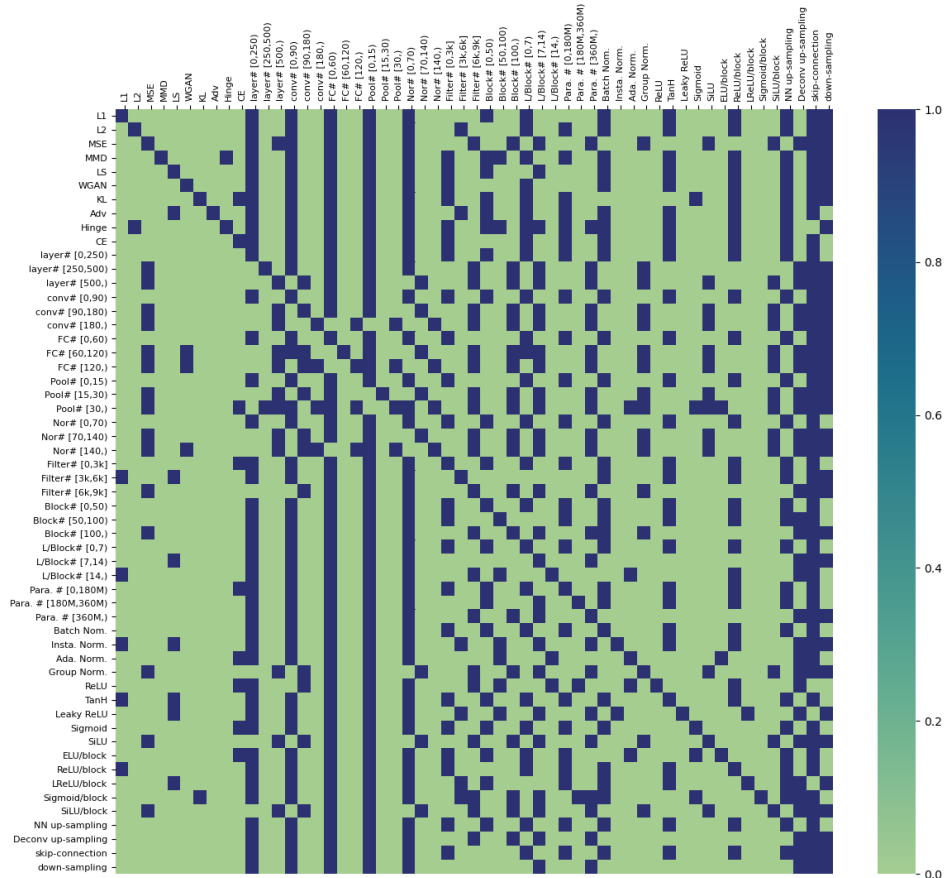


Figure 10: The initial correlation graph A that we construct based on the probability table in Sec. 3.1 of the main paper. The optimum threshold we use is 0.45.

Method	Loss Function		Dis. Archi. Para.		Con. Archi. Para.
	F1 \uparrow	Acc. \uparrow	F1 \uparrow	Acc. \uparrow	L1 error \downarrow
Random GT [2]	0.636	0.716	0.529	0.575	0.184
FEN-PN [2]	0.813	0.792	0.718	0.706	0.149
FEN-PN* [2]	0.801	0.811	0.701	0.708	0.146
GTC w MLP	0.778	0.801	0.689	0.701	0.169
GTC w Stacked -GCN	0.790	0.831	0.698	0.720	0.145
LGPN	0.841	0.833	0.727	0.755	0.130

Table 8: The model parsing performance on RED116. In the last row, our proposed LGPN that contains GTC and GCN Refinement block, which achieves the best model parsing performance in all metrics. [**Key**: GCN refine.: GCN refinement block; **Bold**: best.].

Threshold	Loss Function	Dis. Archi. Para.
	F1/Accuracy \uparrow	
0.35	84.0/83.0	79.2/77.0
0.45	84.6/83.3	79.5/77.5
0.55	84.5/82.8	78.9/77.0
0.65	82.7/82.5	77.0/74.5

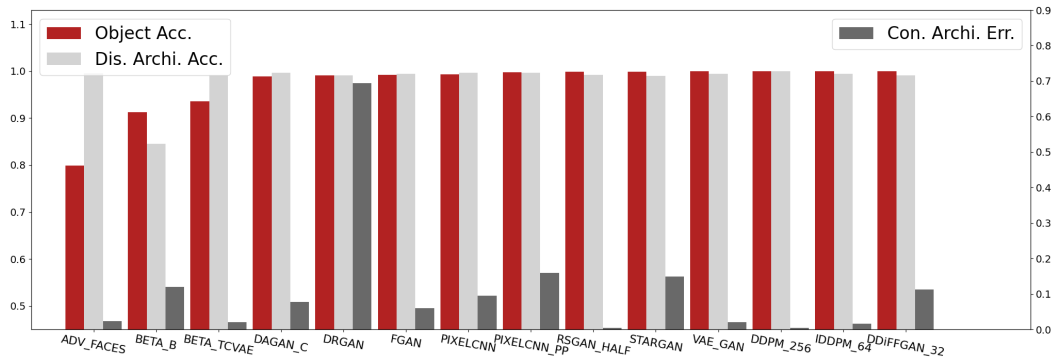
Table 9: More parsing performance with different thresholds constructing the correlation graph **A**.

Method	Test GM	Train GM	Con. Archi. Para. L_1 error \downarrow	Dis. Archi. Para. F1 \uparrow	Loss function F1 \uparrow
FEN-PN	Face	Face	0.139 \pm 0.042	0.729 \pm 0.106	0.788 \pm 0.146
Ours	Face	Face	0.112 \pm 0.028	0.786 \pm 0.116	0.801 \pm 0.134
FEN-PN	Face	Non-Face	0.213 \pm 0.066	0.688 \pm 0.125	0.759 \pm 0.1
Ours	Face	Non-Face	0.139 \pm 0.063	0.694 \pm 0.117	0.771 \pm 0.2
FEN-PN	Face	Full	0.118 \pm 0.046	0.712 \pm 0.129	0.833 \pm 0.136
Ours	Face	Full	0.099 \pm 0.044	0.745 \pm 0.099	0.840 \pm 0.123
FEN-PN	Non-Face	Non-Face	0.118 \pm 0.021	0.794 \pm 0.11	0.864 \pm 0.094
Ours	Non-Face	Face	0.116 \pm 0.016	0.810 \pm 0.102	0.870 \pm 0.092
FEN-PN	Non-Face	Face	0.125 \pm 0.031	0.667 \pm 0.099	0.858 \pm 0.115
Ours	Non-Face	Non-Face	0.100 \pm 0.027	0.692 \pm 0.101	0.882 \pm 0.112
FEN-PN	Non-Face	Full	0.082 \pm 0.045	0.832 \pm 0.046	0.886 \pm 0.061
Ours	Non-Face	Full	0.080 \pm 0.042	0.844 \pm 0.032	0.901 \pm 0.021

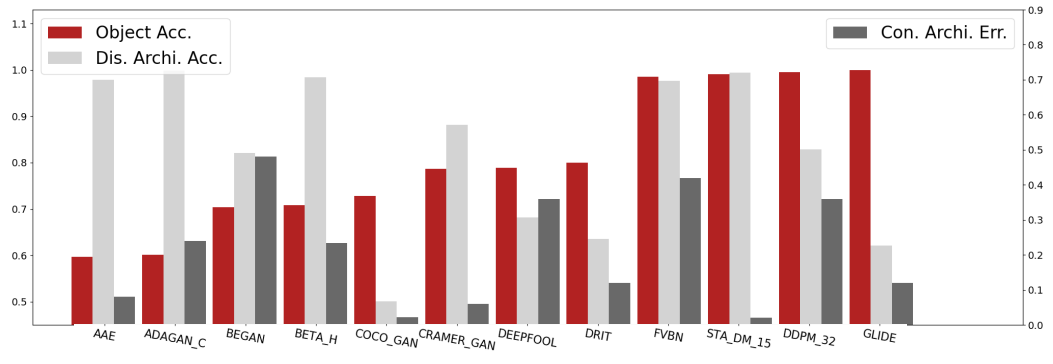
Table 10: Performance comparison across different face and non-face GMs.

Method	Continuous type				Discrete type	
	L_1 error \downarrow	P-value \downarrow	Corr. coef. \uparrow	Coef. of det. \uparrow	F1 score \uparrow	Accuracy \uparrow
Random ground-truth	0.184 \pm 0.019	0.006 \pm 0.001	0.261 \pm 0.181	0.315 \pm 0.095	0.529 \pm 0.078	0.575 \pm 0.097
Mean/mode	0.164 \pm 0.011	0.035 \pm 0.005	0.326 \pm 0.112	0.467 \pm 0.115	0.612 \pm 0.048	0.604 \pm 0.046
No fingerprint	0.170 \pm 0.035	0.017 \pm 0.004	0.738 \pm 0.014	0.605 \pm 0.152	0.700 \pm 0.032	0.663 \pm 0.104
Using one parser	0.161 \pm 0.028	0.032 \pm 0.002	0.226 \pm 0.030	0.512 \pm 0.116	0.607 \pm 0.034	0.593 \pm 0.104
FEN-PN	0.149 \pm 0.019	0.022 \pm 0.007	0.744 \pm 0.098	0.612 \pm 0.161	0.718 \pm 0.036	0.706 \pm 0.040
Ours	0.130 \pm 0.011	N/A	0.833 \pm 0.098	0.732 \pm 0.177	0.743 \pm 0.033	0.755 \pm 0.030

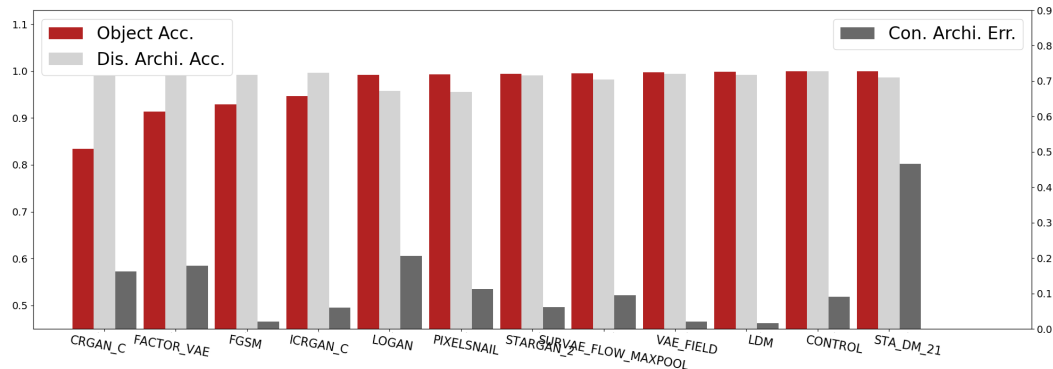
Table 11: Performance of architecture hyperparameters prediction. We use L_1 error, p-value, correlation coefficient, and coefficient of determination for continuous type parameters. For discrete architecture hyperparameters, we use the F1 score and classification accuracy. The first value is the standard deviation across sets, while the second one is across samples. The p-value is estimated for every ours-baseline pair. [**KEYS**: corr.: correlation, coef.: coefficient, det.: determination]



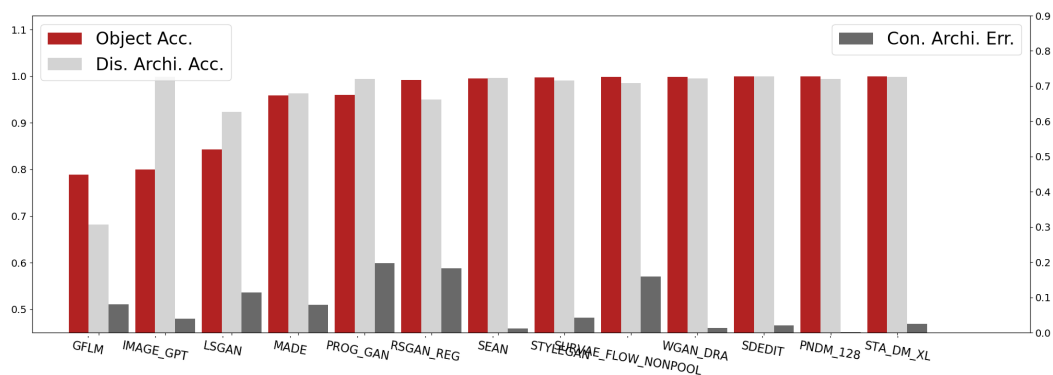
(a)



(b)



(c)



(d)

Figure 11: We report detailed model parsing results on different GMs in each test set. These results include loss function and discrete architecture hyperparameter prediction accuracy, as well as the L1 error on the continuous architecture hyperparameter prediction. Specifically, (a), (b), (c), and (d) are the performance for GMs in the 1st, 2nd, 3rd, and 4th test sets, respectively.

Table 12: Test sets used for evaluation. Each set contains generative models from GAN, DM, VAE, AR (Auto-Regressive), AA (Adversarial Attack), and NF (Normalizing Flow). All test sets contain face and non-face in the image content. [Keys: R means GM is used in the test set of RED116 but is not used in RED140.]

Set 1	Set 2	Set 3	Set 4
ADV_FACES	AAE	BICYCLE_GAN (R)	GFLM
BETA_B	ADAGAN_C	BIGGAN_512 (R)	IMAGE_GPT
BETA_TCVAE	BEGAN	CRGAN_C	LSGAN
BIGGAN_128 (R)	BETA_H	FACTOR_VAE	MADE
DAGAN_C	BIGGAN_256 (R)	FGSM	PIX2PIX (R)
DRGAN	COCOGAN	ICRGAN_C	PROG_GAN
FGAN	CRAMERGAN	LOGAN	RSGAN_REG
PIXEL_CNN	DEEFOOL	MUNIT (R)	SEAN
PIXEL_CNN++	DRIT	PIXEL_SNAIL	STYLE_GAN
RSGAN_HALF	FAST_PIXEL(R)	STARGAN_2	SURVAE_FLOW_NONPOOL
STARGAN	FVBN	SURVAE_FLOW_MAXPOOL	WGAN_DRA
VAEGAN	SRFLOW (R)	VAE_FIELD	YLG (R)
DDPM_256	ADM_G_64	LDM	ADM_G_128
DDPM_64	DDPM_32	CONTROLNET	STABLE_DM_XL
Denoise_GAN_32	GLIDE	STABLE_DM_15	SEDdit

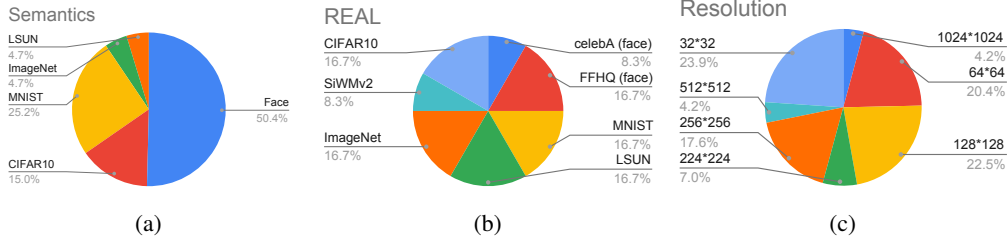


Figure 12: RED140 statistics. (a) The dataset is trained on various image contents or semantics. (b) The real-image category contains many real-image datasets that GMs are trained on [33, 32, 13, 67, 25, 36, 37]. (c) The GM has various image resolutions.

D RED140 Dataset

In this section, we provide an overview of the RED140 dataset, which is used for both model parsing and coordinated attack detection. Note that, for the experiment reported in Tab. ?? of the supplementary, we follow the test sets defined in RED116 [2]. When we construct RED140, we use images from ImageNet, FFHQ, CelebHQ, CIFAR10, and LSUN as the real-images category of RED140. We exclude GM that is not trained in the real-image category of RED140. In addition, both RED116 and RED140 contain various image content and resolution, and the details about RED140 are uncovered in Fig. 12 of the supplementary. For test sets (Tab. 12 of the supplementary), we follow the dataset partition of RED116, excluding the GMs that are trained on real images, which RED140 does have. For example, JFT-300M is used to train BigGAN, so we remove BIGGAN_128, BIGGAN_256 and BIGGAN_512 in the first, second, and third test sets.

E GM Hyperparameter Ground Truth

In this section, we report the ground truth vector of different hyperparameters of each GM contained in the RED140. Specifically, Tab. 13 and Tab. 14 report the loss function ground truth vector for each GM. Tab. 15 and Tab. 16 report the discrete architecture hyperparameter ground truth for each GM. Tab. 17 and Tab. 18 report the continuous architecture hyperparameter ground truth for each GM. The detailed model parsing performance on each GM is reported in the supplementary’s Fig. 11.

Table 13: Ground truth Loss Function feature vector used for prediction of loss type for all GMs. The loss function ground truth is in (Tab. 4).

GM	L_1	L_2	MSE	MMD	LS	WGAN	KL	Adversarial	Hinge	CE
AAE	1	0	0	0	0	0	0	0	0	1
ACGAN	1	0	0	0	0	0	0	0	0	1
ADAGAN_C	0	0	0	0	1	0	0	0	0	1
ADAGAN_P	0	0	0	0	1	0	0	0	0	0
ADM_G_128	0	0	1	0	0	0	0	0	0	0
ADM_G_256	0	0	1	0	0	0	0	0	0	0
ADV_FACES	1	0	1	0	1	0	0	0	0	0
ALAE	0	0	1	0	1	0	0	0	0	0
BEGAN	1	0	0	0	0	0	0	0	0	0
BETA_B	0	0	0	0	0	0	1	0	0	1
BETA_H	0	0	0	0	0	0	1	0	0	1
BETA_TCVAE	1	0	0	0	0	0	1	0	0	1
BGAN	0	0	0	0	1	0	0	0	0	1
BICYCLE_GAN	1	0	1	0	0	0	1	0	0	0
BIGGAN_128	1	0	0	0	0	0	0	0	0	0
BIGGAN_256	1	0	0	0	0	0	0	0	0	0
BIGGAN_512	1	0	0	0	0	0	0	0	0	0
Blended_DM	0	0	1	0	0	0	0	0	0	0
CADGAN	0	0	0	1	0	0	0	0	0	0
CCGAN	0	0	0	0	1	0	0	1	0	0
CGAN	0	0	1	0	1	0	0	0	0	0
CLIPDM	0	0	1	0	0	0	0	0	0	0
COCO_GAN	1	1	0	0	0	1	0	0	1	0
COGAN	0	0	0	0	1	0	0	0	0	0
COLOUR_GAN	1	0	0	0	1	0	0	0	0	0
CONT_ENC	0	1	0	0	1	0	0	0	0	0
CONTRAGAN	1	0	0	0	0	0	0	1	0	1
CONTROLNET	0	0	1	0	0	0	0	0	0	0
COUNCIL_GAN	1	0	1	0	1	0	0	0	0	0
CRAMER_GAN	0	0	0	0	0	1	0	0	0	0
CRGAN_C	1	1	0	0	0	0	0	0	0	1
CRGAN_P	1	1	0	0	0	0	0	0	0	0
CYCLEGAN	1	0	0	0	1	0	0	0	0	0
DAGAN_C	1	0	0	0	0	0	0	0	0	1
DAGAN_P	1	0	0	0	0	0	0	0	0	0
DCGAN	0	0	0	0	0	0	0	0	0	1
DDPM_32	0	0	1	0	0	0	0	0	0	0
DDPM_256	0	0	1	0	0	0	0	0	0	0
DDiFFGAN_32	0	0	1	0	0	1	0	0	0	0
DEEPFOOL	1	1	0	0	0	0	0	0	0	0
DFCVAE	0	1	0	0	0	0	1	0	0	1
DIFFAE_256	0	0	1	0	0	0	0	0	0	0
DIFFAE_LATENT	0	0	1	0	0	0	0	0	0	0
DIFF-ProGAN	0	0	0	0	0	0	1	0	0	0
DIFF-StyleGAN	0	0	0	0	0	0	1	0	0	0
DIFF-ISGEN	0	0	0	0	0	0	1	0	0	0
DISCOGAN	1	0	0	0	1	0	0	0	0	0
DRGAN	0	0	0	0	1	0	0	0	0	1
DRIT	1	0	0	0	1	0	0	0	0	1
DUALGAN	1	0	0	0	0	1	0	0	0	0
EBGAN	0	1	0	0	1	0	0	1	1	0
ESRGAN	1	0	0	0	1	0	0	0	0	0
FACTOR_VAE	1	0	0	0	0	0	1	0	0	1
Fast pixel	0	0	0	0	0	0	0	0	0	1
FFGAN	1	1	0	0	1	0	0	0	0	1
FGAN	0	0	0	0	1	0	0	1	0	0
FGAN_KL	1	0	0	0	0	0	0	0	0	0
FGAN_NEYMAN	0	1	0	0	0	0	0	0	0	0
FGAN_PEARSON	0	0	1	0	0	0	0	0	1	0
FGSM	0	0	0	0	1	0	0	0	0	0
FPGAN	1	1	0	0	1	0	0	0	0	1
FSGAN	1	0	0	0	1	0	0	0	0	1
FVBN	0	0	0	0	0	0	0	0	0	1
GAN_ANIME	1	1	0	0	0	1	0	0	1	0
Gated_pixel_cnn	0	0	0	0	0	0	0	0	0	1
GDWCT	1	0	1	0	0	0	0	0	1	0
GFLM	0	0	1	0	0	0	0	0	0	1
GGAN	1	0	0	0	0	0	0	0	0	0
GLIDE	0	0	1	0	0	0	0	0	0	0
ICRGAN_C	1	1	0	0	0	0	0	0	0	1
ICRGAN_P	1	1	0	0	0	0	0	0	0	0

Table 14: Ground truth Loss Function feature vector used for prediction of loss type for all GMs. The loss function ground truth is in (Tab. 4).

GM	L_1	L_2	MSE	MMD	LS	WGAN	KL	Adversarial	Hinge	CE
IDDPM_32	0	0	1	0	0	0	0	0	0	0
IDDPM_64	0	0	1	0	0	0	0	0	0	0
IDDPM_256	0	0	1	0	0	0	0	0	0	0
ILVER_256	0	0	1	0	0	0	0	0	0	0
Image_GPT	0	0	0	0	0	0	0	0	0	1
INFOGAN	0	0	1	0	1	0	0	0	0	1
LAPGAN	0	0	0	0	1	0	0	0	0	0
LDM	0	0	1	0	0	0	0	0	0	0
LDM_CON	0	0	1	0	0	1	0	0	0	0
Lmconv	0	0	0	0	0	0	0	0	0	1
LOGAN	1	1	0	0	0	0	0	1	0	0
LSGAN	0	0	1	0	0	0	0	0	1	0
MADE	0	0	0	0	0	0	0	0	0	1
MAGAN	0	0	1	0	0	0	0	0	0	0
MEMGAN	0	0	0	0	1	0	0	0	0	0
MMD_GAN	1	0	0	1	0	0	0	0	0	0
MRGAN	0	0	1	0	1	0	0	0	0	0
MSG_STYLE_GAN	0	0	0	0	1	0	0	0	0	0
MUNIT	1	0	0	0	1	0	0	0	0	0
NADE	0	0	0	0	0	0	0	0	0	1
OCFGAN	0	0	0	1	0	0	0	0	1	0
PGD	1	1	0	0	0	0	0	0	0	0
PIX2PIX	1	0	0	0	1	0	0	0	0	0
PixelCNN	0	0	0	0	0	0	0	0	0	1
PixelCNN++	0	0	0	0	0	0	0	0	0	1
PIXELDA	0	0	0	0	1	0	0	0	1	1
PixelSnail	0	0	0	0	0	0	0	0	0	1
PNDM_32	0	0	1	0	0	0	0	0	0	0
PNDM_256	0	0	1	0	0	0	0	0	0	0
PROG_GAN	0	0	0	0	0	1	0	0	1	0
RGAN	0	0	0	0	0	1	0	0	0	0
RSGAN_HALF	0	0	0	0	0	0	0	0	0	1
RSGAN_QUAR	0	0	0	0	0	0	0	0	0	1
RSGAN_REG	0	0	0	0	0	0	0	0	0	1
RSGAN_RES_BOT	0	0	0	0	0	0	0	0	0	1
RSGAN_RES_HALF	0	0	0	0	0	0	0	0	0	1
RSGAN_RES_QUAR	0	0	0	0	0	0	0	0	0	1
RSGAN_RES_REG	0	0	0	0	0	0	0	0	0	1
SAGAN	0	0	0	0	1	0	0	0	0	0
SCOREDIFF_256	0	0	1	0	0	0	0	0	0	0
SDEdit_256	0	0	1	0	0	0	0	0	0	0
SEAN	1	0	0	0	1	0	0	0	0	0
SEMANTIC	0	1	0	0	1	0	0	0	0	0
SGAN	0	0	0	0	1	0	0	0	0	1
SNGAN	0	0	0	0	1	0	0	1	0	0
SOFT_GAN	0	0	0	0	1	0	0	0	0	0
SRFLOW	1	0	0	0	0	0	0	0	0	1
SRRNET	0	1	1	0	1	0	0	0	0	1
STANDARD_VAE	0	0	0	0	0	0	1	0	0	1
STARGAN	1	0	0	0	1	0	0	0	0	1
STARGAN_2	1	0	0	0	1	0	0	0	0	0
STA_DM_15	0	0	1	0	0	0	0	0	0	0
STA_DM_21	0	0	1	0	0	0	0	0	0	0
STA_DM_XL	0	0	1	0	0	0	0	0	0	0
STGAN	1	0	0	0	1	1	0	0	0	0
STYLEGAN	0	1	0	0	0	1	0	0	0	0
STYLEGAN_2	0	1	0	0	1	0	0	0	1	0
STYLEGAN2_ADA	0	1	0	1	1	0	0	0	1	0
SURVAE_FLOW_MAXPOOL	0	0	0	0	0	0	1	0	0	1
SURVAE_FLOW_NONPOOL	0	0	0	0	0	0	1	0	0	1
TPGAN	1	0	0	0	0	1	0	0	0	0
UGAN	0	0	0	0	1	0	0	0	0	0
UNIT	0	0	0	0	1	0	1	0	0	0
VAE_field	0	0	0	0	0	0	1	0	0	1
VAE_flow	0	0	0	0	0	0	1	0	0	1
VAEGAN	1	0	0	0	1	0	1	0	0	0
VDVAE	0	0	0	0	0	0	1	0	0	1
WGAN	0	0	0	0	0	1	0	0	0	0
WGAN_DRA	0	0	1	0	0	1	0	0	0	0
WGAN_WC	0	0	0	0	0	1	0	0	0	0
WGANGP	0	1	0	0	0	1	0	0	0	0
YLG	0	0	0	0	0	1	0	0	0	0

Table 15: Ground truth feature vector used for prediction of Discrete Architecture Hyperparameters for all GMs. The discrete architecture hyperparameter ground truth is defined in (Tab. 5). **A — D** are Batch Norm., Instance Norm., Adaptive Instance Norm., and Group Norm., respectively. **E — I** are non-linearity in the last layer, and they are ReLU, Tanh, Leaky_ReLu, Sigmoid, and SiLU. **J — N** are non-linearity in the last block, and they are ELU, ReLU, Leaky_ReLu, Sigmoid, and SiLU. **O** and **P** are Nearest Neighbour and Deconvolution Upsampling. **Q** and **L** are Skip Connection and Downsampling.

GM	A	B	C	D	E	F	G	H	I	J	K	L	M	N	O	P	Q	L	
AAE	1	0	0	0	0	1	0	0	0	1	0	0	0	0	1	0	1	0	
ACGAN	1	0	0	0	0	1	0	0	0	0	1	0	0	0	0	1	0	1	0
ADAGAN_C	1	0	0	0	0	1	0	0	0	0	1	0	0	0	0	1	0	1	0
ADAGAN_P	1	0	0	0	0	1	0	0	0	0	1	0	0	0	0	1	0	1	0
ADM_G_128	0	0	1	0	0	0	0	1	0	0	0	0	0	1	1	0	1	1	1
ADM_G_256	0	0	1	0	0	0	0	1	0	0	0	0	0	1	1	0	1	1	1
ADV_FACES	0	1	0	0	0	1	0	0	0	0	1	0	0	0	1	0	1	0	0
ALAE	0	1	0	0	0	0	1	0	0	0	0	1	0	0	0	1	0	1	0
BEGAN	1	0	0	0	0	1	0	0	0	1	0	0	0	0	1	0	0	0	0
BETA_B	0	0	0	0	0	0	0	1	0	0	1	0	0	0	1	0	1	1	1
BETA_H	0	0	0	0	0	0	0	1	0	0	1	0	0	0	1	0	1	1	1
BETA_TCVAE	0	0	0	0	0	0	0	1	0	0	1	0	0	0	1	0	1	1	1
BGAN	1	0	0	0	0	1	0	0	0	0	0	1	0	0	0	1	0	0	0
BICYCLE_GAN	1	0	0	0	0	1	0	0	0	0	1	0	0	0	1	0	0	0	0
BIGGAN_128	1	0	0	0	0	1	0	0	0	0	1	0	0	0	0	1	1	1	1
BIGGAN_256	1	0	0	0	0	1	0	0	0	0	1	0	0	0	0	1	1	1	1
BIGGAN_512	1	0	0	0	0	1	0	0	0	0	1	0	0	0	0	1	1	1	1
Blended_DM	0	0	0	1	0	0	0	0	1	0	0	0	0	1	0	1	1	1	1
CADGAN	1	0	0	0	0	1	0	0	0	0	1	0	0	0	1	0	1	1	1
CCGAN	1	0	0	0	0	1	0	0	0	0	1	0	0	0	0	1	1	1	1
CGAN	1	0	0	0	0	1	0	0	0	0	0	1	0	0	1	0	0	0	0
CLIPDM	0	0	0	1	0	0	0	0	0	0	0	0	0	0	0	1	1	1	1
COCO_GAN	1	0	0	0	0	1	0	0	0	0	1	0	0	0	1	0	0	0	0
COGAN	1	0	0	0	0	1	0	0	0	0	0	1	0	0	1	0	1	1	1
COLOUR_GAN	1	0	0	0	0	1	0	0	0	0	1	0	0	0	1	0	1	1	1
CONT_ENC	1	0	0	0	0	1	0	0	0	0	0	1	0	0	1	0	1	1	1
CONTRAGAN	1	0	0	0	0	1	0	0	0	0	1	0	0	0	1	0	1	0	0
CONTROLNET	0	0	0	1	0	0	0	1	0	0	1	0	0	0	1	0	1	1	1
COUNCIL_GAN	0	1	0	0	0	1	0	0	0	0	1	0	0	0	1	0	1	0	0
CRAMER_GAN	1	0	0	0	0	1	0	0	0	0	1	0	0	0	1	0	1	0	0
CRGAN_C	1	0	0	0	0	1	0	0	0	0	1	0	0	0	1	0	1	0	0
CRGAN_P	1	0	0	0	0	1	0	0	0	0	1	0	0	0	1	0	1	0	0
CYCLEGAN	0	1	0	0	0	1	0	0	0	0	1	0	0	0	0	1	1	1	1
DAGAN_C	1	0	0	0	0	1	0	0	0	0	1	0	0	0	1	0	1	0	0
DAGAN_P	1	0	0	0	0	1	0	0	0	0	1	0	0	0	1	0	1	0	0
DCGAN	1	0	0	0	0	1	0	0	0	0	1	0	0	0	1	0	1	0	0
DDiFFGAN_32	1	0	0	0	0	0	0	1	0	0	0	0	0	1	1	0	1	1	1
DDPM_32	1	0	0	0	0	0	0	1	0	0	1	0	0	0	1	0	1	1	1
DDPM_256	1	0	0	0	0	0	0	1	0	0	1	0	0	0	1	0	1	1	1
DEEPOOL	0	0	1	0	1	0	0	0	0	0	1	0	0	0	0	1	0	0	0
DFCVAE	1	0	0	0	0	0	0	1	0	0	0	1	0	0	1	0	0	1	1
DIFF_ISGEN	0	0	0	0	0	0	1	0	0	0	0	0	1	0	1	0	0	0	0
DIFF_PGAN	0	0	0	0	0	0	1	0	0	0	0	0	1	0	1	0	0	0	0
DIFF_SGAN	0	0	0	0	0	0	1	0	0	0	0	0	1	0	1	0	0	0	0
DIFFAE	1	0	0	0	0	0	0	1	0	0	0	0	0	1	1	0	1	1	1
DIFFAE_LATENT	1	0	0	0	0	0	0	1	0	0	0	0	0	1	1	0	1	1	1
DISCOGAN	0	1	0	0	0	1	0	0	0	0	0	0	1	0	0	1	1	1	1
DRGAN	1	0	0	0	0	1	0	0	0	1	0	0	0	0	1	0	1	1	1
DRIT	0	1	0	0	0	1	0	0	0	0	1	0	0	0	0	1	1	1	1
DUALGAN	1	0	0	0	0	1	0	0	0	0	1	0	0	0	1	0	0	0	0
EBGAN	1	0	0	0	0	1	0	0	0	0	0	1	0	0	1	0	0	1	0
ESRGAN	0	0	1	0	0	0	1	0	0	0	0	1	0	0	0	1	0	0	0
FACTOR_VAE	0	0	0	0	0	0	0	1	0	0	1	0	0	0	1	0	1	1	1
FASTPIXEL	1	0	0	0	0	0	0	1	0	1	0	0	0	0	1	0	1	0	0
FFGAN	1	0	0	0	0	1	0	0	0	0	1	0	0	0	0	1	1	1	1
FGAN	1	0	0	0	0	0	0	1	0	0	1	0	0	0	1	0	1	0	0
FGAN_KL	1	0	0	0	0	0	0	1	0	0	1	0	0	0	1	0	1	0	0
FGAN_NEYMAN	1	0	0	0	0	0	0	1	0	0	1	0	0	0	1	0	1	0	0
FGAN_PEARSON	1	0	0	0	0	0	0	1	0	0	1	0	0	0	1	0	1	0	0
FGSM	0	0	1	0	1	0	0	0	0	0	1	0	0	0	0	1	0	0	0
FPGAN	0	1	0	0	0	1	0	0	0	0	1	0	0	0	1	0	0	0	1
FSGAN	1	0	0	0	1	0	0	0	0	0	1	0	0	0	0	1	1	1	1
FVBN	0	0	1	0	0	0	0	1	0	1	0	0	0	0	1	0	1	0	0
GAN_ANIME	0	1	0	0	0	1	0	0	0	0	1	0	0	0	1	0	1	1	1
GATED_PIXEL_CNN	0	0	1	0	0	0	0	1	0	0	0	1	0	0	0	1	1	0	0
GDWCT	0	1	0	0	0	1	0	0	0	0	1	0	0	0	1	0	0	1	0
GFLM	0	0	1	0	1	0	0	0	0	0	1	0	0	0	0	1	0	0	0
GGAN	1	0	0	0	0	1	0	0	0	0	1	0	0	0	1	0	1	1	1
GLIDE	1	0	0	0	0	0	0	1	0	0	0	0	0	1	1	0	1	1	1

Table 16: Ground truth feature vector used for prediction of Discrete Architecture Hyperparameters for all GMs. The discrete architecture hyperparameter ground truth is defined in (Tab. 5). **A — D** are Batch Norm., Instance Norm., Adaptive Instance Norm., and Group Norm., respectively. **E — I** are non-linearity in the last layer and they are ReLU, Tanh, Leaky_ReLu, Sigmoid, and SiLU. **J — N** are non-linearity in the last block and they are ELU, ReLU, Leaky_ReLu, Sigmoid, and SiLU. **O** and **P** are Nearest Neighbour and Deconvolution Upsampling. **Q** and **L** are Skip Connection and Downsampling.

GM	A	B	C	D	E	F	G	H	I	J	K	L	M	N	O	P	Q	L
ICRGAN_C	1	0	0	0	0	1	0	0	0	0	1	0	0	0	1	0	1	0
ICRGAN_P	1	0	0	0	0	1	0	0	0	0	1	0	0	0	1	0	1	0
IDDPM_32	0	0	1	0	0	0	0	1	0	0	0	0	0	1	1	0	1	1
IDDPM_64	0	0	1	0	0	0	0	1	0	0	0	0	0	1	1	0	1	1
IDDPM_256	0	0	1	0	0	0	0	1	0	0	0	0	0	1	1	0	1	1
IMAGE_GPT	1	0	0	0	0	0	0	1	0	0	0	1	0	0	0	1	1	1
INFOGAN	1	0	0	0	0	1	0	0	0	0	0	1	0	0	1	0	0	1
ILVER_256	0	0	0	1	0	0	0	0	0	0	0	0	0	0	0	1	1	1
LAPGAN	0	0	1	0	0	1	0	0	0	0	1	0	0	0	0	1	1	0
LDM	1	0	0	0	0	0	0	1	0	0	0	0	0	1	1	0	1	1
LDM_CON	1	0	0	0	0	0	0	1	0	0	0	0	0	1	1	0	1	1
LMCONV	0	0	1	0	0	0	0	1	0	1	0	0	0	0	0	1	1	1
LOGAN	1	0	0	0	0	1	0	0	0	0	1	0	0	0	1	0	1	0
LSGAN	1	0	0	0	0	1	0	0	0	0	1	0	0	0	1	0	0	0
MADE	0	0	1	0	0	0	0	1	0	1	0	0	0	0	1	0	1	0
MAGAN	1	0	0	0	0	1	0	0	0	0	1	0	0	0	1	0	1	0
MEMGAN	1	0	0	0	0	1	0	0	0	0	1	0	0	0	1	0	1	0
MMD_GAN	1	0	0	0	0	1	0	0	0	0	1	0	0	0	1	0	1	0
MRGAN	1	0	0	0	0	1	0	0	0	0	1	0	0	0	1	0	1	0
MSG_STYLE_GAN	0	1	0	0	0	0	1	0	0	0	0	1	0	0	0	1	0	1
MUNIT	0	1	0	0	1	0	0	0	0	1	0	0	0	0	0	1	1	1
NADE	0	0	1	0	0	0	0	1	0	1	0	0	0	0	1	0	1	0
OCFGAN	1	0	0	0	0	1	0	0	0	0	1	0	0	0	1	0	1	0
PGD	0	0	1	0	1	0	0	0	0	0	1	0	0	0	0	1	0	0
PIX2PIX	0	1	0	0	0	1	0	0	0	0	0	1	0	0	0	1	1	1
PIXELCNN	1	0	0	0	0	0	0	1	0	1	0	0	0	0	1	0	1	0
PIXELCNN_PP	0	0	1	0	0	0	0	1	0	1	0	0	0	0	0	1	1	1
PIXELDA	1	0	0	0	0	1	0	0	0	0	1	0	0	0	0	1	0	0
PIXELSNAIL	0	0	1	0	1	0	0	0	0	0	0	0	1	0	1	0	1	0
PNDM_32	0	0	0	1	0	0	0	0	1	0	0	0	0	1	0	1	1	1
PNDM_256	0	0	0	1	0	0	0	0	1	0	0	0	0	1	0	1	1	1
PROG_GAN	1	0	0	0	0	0	0	1	0	0	0	0	1	0	1	0	0	1
RGAN	1	0	0	0	0	1	0	0	0	0	0	1	0	0	1	0	0	1
RSGAN_HALF	1	0	0	0	0	1	0	0	0	0	1	0	0	0	1	0	1	0
RSGAN_QUAR	1	0	0	0	0	1	0	0	0	0	1	0	0	0	1	0	1	0
RSGAN_REG	1	0	0	0	0	1	0	0	0	0	1	0	0	0	1	0	1	0
RSGAN_RES_BOT	1	0	0	0	0	1	0	0	0	0	1	0	0	0	0	1	1	0
RSGAN_RES_HALF	1	0	0	0	0	1	0	0	0	0	1	0	0	0	0	1	1	0
RSGAN_RES_QUAR	1	0	0	0	0	1	0	0	0	0	1	0	0	0	0	1	1	0
RSGAN_RES_REG	1	0	0	0	0	1	0	0	0	0	1	0	0	0	0	1	1	0
SAGAN	1	0	0	0	0	1	0	0	0	0	0	1	0	0	1	0	0	0
SCOREDIFF_256	0	0	0	1	0	0	0	0	0	0	0	0	0	0	0	1	1	1
SDEDIT	0	0	0	1	0	0	0	0	1	0	1	0	0	0	1	0	1	1
SEAN	0	0	0	0	0	1	0	0	0	0	1	0	0	0	1	0	1	0
SEMANTIC	0	1	0	0	0	1	0	0	0	0	1	0	0	0	1	0	0	1
SGAN	1	0	0	0	0	1	0	0	0	0	0	1	0	0	0	1	0	0
SNGAN	1	0	0	0	0	1	0	0	0	0	1	0	0	0	1	0	1	0
SOFT_GAN	1	0	0	0	0	1	0	0	0	0	0	1	0	0	1	0	0	0
SRRFLOW	0	0	1	0	0	0	1	0	0	1	0	0	0	0	0	1	0	0
SRRNET	1	0	0	0	0	1	0	0	0	0	1	0	0	0	1	0	1	1
STANDARD_VAE	0	0	0	0	0	0	0	1	0	0	1	0	0	0	1	0	1	1
STA_DM_15	1	0	0	0	0	0	0	1	0	0	1	0	0	0	1	0	1	1
STA_DM_21	1	0	0	0	0	0	0	1	0	0	1	0	0	0	1	0	1	1
STA_DM_XL	1	0	0	0	0	0	0	1	0	0	1	0	0	0	1	0	1	1
STARGAN	0	1	0	0	0	1	0	0	0	0	1	0	0	0	1	0	0	1
STARGAN_2	0	1	0	0	0	0	1	0	0	0	0	1	0	0	1	0	0	1
STGAN	1	0	0	0	0	1	0	0	0	0	0	1	0	0	0	1	1	1
STYLEGAN	0	1	0	0	0	0	1	0	0	0	0	1	0	0	0	1	0	1
STYLEGAN_2	0	1	0	0	0	0	1	0	0	0	0	1	0	0	0	1	0	1
STYLEGAN_ADA	0	1	0	0	0	0	1	0	0	0	0	1	0	0	0	1	0	1
SURVAE_M	0	0	1	0	1	0	0	0	0	1	0	0	0	0	1	0	0	0
SURVAE_N	0	0	1	0	1	0	0	0	0	1	0	0	0	0	1	0	0	0
TPGAN	1	0	0	0	0	0	0	1	0	0	0	0	1	0	1	0	1	1
UGAN	1	0	0	0	0	0	0	1	0	0	1	0	0	0	1	0	1	0
UNIT	0	1	0	0	0	1	0	0	0	0	1	0	0	0	0	1	1	1
VAE_FIELD	0	0	1	0	0	0	0	1	0	1	0	0	0	0	1	0	0	0
VAE_FLOW	0	0	1	0	0	0	0	1	0	1	0	0	0	0	1	0	0	0
VAE_GAN	1	0	0	0	0	1	0	0	0	0	1	0	0	0	1	0	0	1
VDVAE	0	0	1	0	1	0	0	0	0	0	0	1	0	0	0	1	1	1
WGAN	1	0	0	0	0	1	0	0	0	0	1	0	0	0	1	0	0	0
WGAN_DRA	1	0	0	0	0	1	0	0	0	0	1	0	0	0	1	0	1	0
WGAN_WC	1	0	0	0	0	1	0	0	0	0	1	0	0	0	1	0	1	0
WGAN_GP	1	0	0	0	0	1	0	0	0	0	1	0	0	0	1	0	0	0
YLG	1	0	0	0	0	1	0	0	0	0	1	0	0	0	0	1	1	1

Table 17: Ground truth feature vector used for prediction of Continuous Architecture Hyperparameters for all GMs. The discrete architecture hyperparameter ground truth is defined in (Tab. 6). F1: # layers, F2: # convolutional layers, F3: # fully connected layers, F4: # pooling layers, F5: # normalization layers, F6: #filters, F7: # blocks, F8:# layers per block, and F9: # parameters.

GM	Layer #	Conv. #	FC #	Pool #	Norm. #	Filter #	Block #	Block Layer #	Para. #
AAE	9	0	7	0	2	0	0	0	1,593,378
ACGAN	18	10	1	0	7	2,307	5	3	4,276,739
ADAGAN_C	35	14	13	1	7	4,131	9	3	9,416,196
ADAGAN_P	35	14	13	1	7	4,131	9	3	9,416,196
ADM_G_128	223	90	37	8	88	N/A	34	7	421,529,606
ADM_G_256	266	107	45	11	103	N/A	39	7	553,838,086
ADV_FACES	45	23	1	1	20	2,627	4	6	30,000,000
ALAE	33	25	8	0	0	4,094	3	8	50,200,000
BEGAN	10	9	1	0	0	515	2	4	7,278,472
BETA_B	7	4	3	0	0	99	1	3	469,173
BETA_H	7	4	3	0	0	99	1	3	469,173
BETA_TCVAE	7	4	3	0	0	99	1	3	469,173
BGAN	8	0	5	0	3	0	2	3	1,757,412
BICYCLE_GAN	25	14	1	0	10	4,483	2	10	23,680,256
BIGGAN_128	63	21	1	0	41	6,123	6	10	50,400,000
BIGGAN_256	75	25	1	0	49	7,215	6	12	55,900,000
BIGGAN_512	87	29	1	0	57	8,365	6	14	56,200,000
Blended_DM	266	107	45	11	103	N/A	39	7	553,838,086
CADGAN	8	4	1	0	3	451	3	2	3,812,355
CCGAN	22	12	0	0	10	3,203	2	9	29,257,731
CGAN	8	0	5	0	3	0	2	3	1,757,412
COCO_GAN	19	9	1	0	9	2,883	3	4	50,000,000
COGAN	9	5	0	0	4	259	2	2	1,126,790
COLOUR_GAN	19	10	0	0	9	2,435	2	9	19,422,404
CONT_ENC	19	11	0	0	8	5,987	2	8	40,401,187
CONTRAGAN	35	14	13	1	7	4,131	9	3	9,416,196
CONTROLNET	427	121	132	0	174	N/A	56	7	39,726,979
COUNCIL_GAN	62	30	3	0	29	6,214	2	10	69,616,944
CLIPDM	226	120	34	0	72	N/A	38	3	113,673,219
CRAMER_GAN	9	4	1	0	4	454	2	3	9,681,284
CRGAN_C	35	14	13	1	7	4,131	9	3	9,416,196
CRGAN_P	35	14	13	1	7	4,131	9	3	9,416,196
CYCLEGAN	47	24	0	0	23	2,947	4	9	11,378,179
DAGAN_C	35	14	13	1	7	4,131	9	3	9,416,196
DAGAN_P	35	14	13	1	7	4,131	9	3	9,416,196
DCGAN	9	4	1	0	4	454	2	3	9,681,284
DDIFFGAN_32	289	80	91	0	118	N/A	40	2	48,432,515
DDPM_32	164	89	24	0	51	N/A	28	7	35,746,307
DDPM_256	225	120	34	0	71	N/A	39	7	113,673,219
DEEFOOL	95	92	1	2	0	7,236	4	10	22,000,000
DFCVAE	45	22	2	0	21	4,227	4	7	2,546,234
DIFF_ISGEN	88	24	56	0	8	N/A	8	6	30,276,583
DIFF_PGAN	45	20	0	3	13	N/A	11	4	105,684,175
DIFF_SGAN	48	20	28	0	8	N/A	8	6	24,767,458
DIFFAE	712	263	171	45	233	N/A	118	7	336,984,582
DIFFAE_LATENT	717	264	172	46	235	N/A	155	6	445,203,974
DISCOGAN	21	12	0	0	9	3,459	2	9	29,241,731
DRGAN	44	28	1	1	14	4,481	3	8	18,885,068
DRIT	19	10	0	0	9	1,793	4	3	9,564,170
DUALGAN	25	14	1	0	10	4,483	2	10	23,680,256
EBGAN	6	3	1	0	2	195	2	2	738,433
ESRGAN	66	66	0	0	0	4,547	5	4	7,012,163
FACTOR_VAE	7	4	3	0	0	99	1	3	469,173
Fast pixel	17	9	0	0	8	768	2	8	4,600,000
FFGAN	39	19	1	1	19	3,261	0	0	50,000,000
FGAN	5	0	3	0	2	0	2	2	2,256,401
FGAN_KL	5	0	3	0	2	0	2	2	2,256,401
FGAN_NEYMAN	5	0	3	0	2	0	2	2	2,256,401
FGAN_PEARSON	5	0	3	0	2	0	2	2	2,256,401
FGSM	95	92	1	2	0	7,236	4	10	22,000,000
FPGAN	23	12	0	0	11	2,179	2	6	53,192,576
FSGAN	37	20	0	1	16	2,863	4	8	94,669,184
FVBN	28	0	28	0	0	0	1	1	307,721
GAN_ANIME	25	18	0	0	7	2,179	4	6	8,467,854
Gated_pixel_cnn	32	32	0	0	0	5,433	3	10	3,364,161
GDWCT	79	27	40	1	11	5,699	2	4	51,965,832
GFLM	95	92	1	2	0	7,236	4	10	22,000,000
GGAN	8	4	1	0	3	451	3	2	3,812,355
GLIDE	331	93	103	6	129	N/A	74	5	385,030,726
ICRGAN_C	35	14	13	1	7	4,131	9	3	9,416,196
ICRGAN_P	35	14	13	1	7	4,131	9	3	9,416,196

Table 18: Ground truth feature vector used for prediction of Continuous Architecture Hyperparameters for all GMs. The discrete architecture hyperparameter ground truth is defined in (Tab. 6). F1: # layers, F2: # convolutional layers, F3: # fully connected layers, F4: # pooling layers, F5: # normalization layers, F6: #filters, F7: # blocks, F8:# layers per block, and F9: # parameters.

GM	Layer #	Conv. #	FC #	Pool #	Norm. #	Filter #	Block #	Block Layer #	Para. #
IDDDPM_32	193	85	32	0	76	N/A	45	2	52, 546, 438
IDDDPM_64	195	87	32	0	76	N/A	45	2	27, 3049, 350
IDDDPM_256	201	96	34	0	71	N/A	40	5	113, 676, 678
ILVER_256	266	107	45	11	103	N/A	39	7	553, 838, 086
Image_GPT	59	42	0	0	17	4, 673	7	8	401, 489
INFOGAN	7	3	1	0	3	195	2	2	1, 049, 985
LAPGAN	11	6	5	0	0	262	4	2	2, 182, 857
LDM	255	127	24	0	104	N/A	65	4	329, 378, 945
LDM_CON	503	159	184	8	152	N/A	65	8	456, 755, 873
Lmconv	105	60	10	35	0	7, 156	15	5	46, 000, 000
LOGAN	35	14	13	1	7	4, 131	9	3	9, 416, 196
LSGAN	9	5	0	0	4	1, 923	2	4	23, 909, 265
MADE	2	0	2	0	0	0	1	2	12552784
MAGAN	9	5	0	0	4	963	2	3	11, 140, 934
MEMGAN	14	7	1	0	6	1, 155	3	4	4, 128, 515
MMD_GAN	9	4	1	0	4	454	2	3	9, 681, 284
MRGAN	9	4	1	0	4	451	3	2	15, 038, 350
MSG_STYLE_GAN	33	25	8	0	0	4, 094	3	8	50, 200, 000
MUNIT	18	15	0	0	3	3, 715	2	6	10, 305, 035
NADE	1	0	1	0	0	0	1	1	785, 284
OCFGAN	9	4	1	0	4	454	2	3	9, 681, 284
PGD	95	92	1	2	0	7, 236	4	10	22, 000, 000
PIX2PIX	29	16	0	0	13	5, 507	2	13	54, 404, 099
PixelCNN	17	9	0	0	8	768	2	8	4, 600, 000
PixelCNN++	105	60	10	35	0	7, 156	15	5	46, 000, 000
PIXELDA	27	14	1	0	12	835	4	6	483, 715
PixelSnail	90	90	0	0	0	4, 051	3	10	40, 000, 000
PNDM_32	164	89	24	0	51	N/A	28	7	35, 746, 307
PNDM_256	266	107	45	11	103	N/A	39	7	553, 838, 086
PROG_GAN	26	25	1	0	0	4, 600	3	8	46, 200, 000
RGAN	7	3	1	0	3	195	2	2	1, 049, 985
RSGAN_HALF	8	4	1	0	3	899	3	2	13, 129, 731
RSGAN_QUAR	8	4	1	0	3	451	3	2	3, 812, 355
RSGAN_REG	8	4	1	0	3	1, 795	3	2	48, 279, 555
RSGAN_RES_BOT	15	7	1	0	7	963	3	4	758, 467
RSGAN_RES_HALF	15	7	1	0	7	1, 155	3	4	1, 201, 411
RSGAN_RES_QUAR	15	7	1	0	7	579	3	4	367, 235
RSGAN_RES_REG	15	7	1	0	7	2, 307	3	4	4, 270, 595
SAGAN	11	6	1	0	4	139	2	4	16, 665, 286
SEAN	19	16	0	0	0	5, 062	2	7	266, 907, 367
SEMANTIC	23	12	0	0	11	2, 179	2	6	53, 192, 576
SGAN	7	3	1	0	3	195	2	2	1, 049, 985
SCOREDIFF_256 225	120	34	0	11	71	N/A	39	7	113, 673, 219
SDEdit	226	120	34	0	72	N/A	38	3	113, 673, 219
SNGAN	23	11	1	0	11	3, 871	4	5	10, 000, 000
SOFT_GAN	8	0	5	0	3	0	2	3	1, 757, 412
SRRFLOW	66	66	0	0	2	4, 547	5	4	7, 012, 163
SRRNET	74	36	1	0	37	2, 819	4	16	4, 069, 955
STANDARD_VAE	7	4	3	0	0	99	1	3	469, 173
STARGAN	23	12	0	0	11	2, 179	2	6	53, 192, 576
STARGAN_2	67	26	12	4	25	4, 188	4	12	94, 008, 488
STA_DM_15	503	159	184	8	152	N/A	65	8	456, 755, 873
STA_DM_21	503	159	184	8	152	N/A	65	8	456, 755, 873
STA_DM_XL	601	184	201	12	185	N/A	74	9	618, 997, 638
STGAN	19	10	0	0	9	2, 953	2	5	25, 000, 000
STYLEGAN	33	25	8	0	0	4, 094	3	8	50, 200, 000
STYLEGAN_2	33	25	8	0	0	4, 094	3	8	59, 000, 000
STYLEGAN2_ADA	33	25	8	0	0	4, 094	3	8	59, 000, 000
SURVAE_FLOW_MAX	95	90	0	5	0	6, 542	2	20	25, 000, 000
SURVAE_FLOW_NON	90	90	0	0	0	6, 542	2	20	25, 000, 000
TPGAN	45	31	2	1	11	5, 275	0	0	27, 233, 200
UGAN	9	4	1	0	4	771	2	3	4, 850, 692
UNIT	43	22	0	0	21	4, 739	4	8	13, 131, 779
VAE_field	6	0	6	0	0	0	1	3	300, 304
VAE_flow	14	0	14	0	0	0	2	4	760, 448
VAEGAN	17	7	2	0	8	867	2	6	26, 396, 740
VDVAE	48	42	0	6	0	3, 502	3	13	41, 000, 000
WGAN	9	5	0	0	4	1, 923	2	4	23, 909, 265
WGAN_DRA	18	10	1	0	7	2, 307	5	3	4, 276, 739
WGAN_WC	18	10	1	0	7	2, 307	5	3	4, 276, 739
WGANP	9	5	0	0	4	1, 923	2	4	23, 905, 841
YLG	33	20	1	2	10	5, 155	5	5	42, 078, 852